Deep-Sea Research II 56 (2009) 68–86

Contents lists available at ScienceDirect

Deep-Sea Research II

journal homepage: www.elsevier.com/locate/dsr2

Preparing to predict: The Second Autonomous Ocean Sampling Network (AOSN-II) experiment in the Monterey Bay

S.R. Ramp [a,*], R.E. Davis [b], N.E. Leonard [c], I. Shulman [d], Y. Chao [e], A.R. Robinson [f], J. Marsden [g], P.F.J. Lermusiaux [h], D.M. Fratantoni [i], J.D. Paduan [j], F.P. Chavez [a], F.L. Bahr [j], S. Liang [f], W. Leslie [f], Z. Li [e]

[a] Monterey Bay Aquarium Research Institute, 7700 Sandholdt Road, Moss Landing, CA 95039, USA
[b] Scripps Institution of Oceanography, La Jolla, CA, USA
[c] Department of Mechanical Engineering, Princeton University, Princeton, NJ, USA
[d] Naval Research Laboratory, Stennis Space Center, MS, USA
[e] Jet Propulsion Laboratory, Pasadena, CA, USA
[f] Harvard University, Cambridge, MA, USA
[g] California Institute of Technology, Pasadena, CA, USA
[h] Massachusetts Institute of Technology, Cambridge, MA, USA
[i] Woods Hole Oceanographic Institution, Woods Hole, MA, USA
[j] Naval Postgraduate School, Monterey, CA, USA

ARTICLE INFO

Article history:
Accepted 14 August 2008
Available online 25 October 2008

Keywords:
Ocean circulation
Ocean heat budget
Ocean winds
Ocean temperature
Salinity
Density

ABSTRACT

The Autonomous Ocean Sampling Network Phase Two (AOSN-II) experiment was conducted in and offshore from the Monterey Bay on the central California coast during July 23–September 6, 2003. The objective of the experiment was to learn how to apply new tools, technologies, and analysis techniques to adaptively sample the coastal ocean in a manner demonstrably superior to traditional methodologies, and to use the information gathered to improve predictive skill for quantities of interest to end-users. The scientific goal was to study the upwelling/relaxation cycle near an open coastal bay in an eastern boundary current region, particularly as it developed and spread from a coastal headland. The suite of observational tools used included a low-flying aircraft, a fleet of underwater gliders, including several under adaptive autonomous control, and propeller-driven AUVs in addition to moorings, ships, and other more traditional hardware. The data were delivered in real time and assimilated into the Harvard Ocean Prediction System (HOPS), the Navy Coastal Ocean Model (NCOM), and the Jet Propulsion Laboratory implementation of the Regional Ocean Modeling System (JPL/ROMS).

Two upwelling events and one relaxation event were sampled during the experiment. The upwelling in both cases began when a pool of cold water less than 13 °C appeared near Cape Año Nuevo and subsequently spread offshore and southward across the bay as the equatorward wind stress continued. The primary difference between the events was that the first event spread offshore and southward, while the second event spread only southward and not offshore. The difference is attributed to the position and strength of meanders and eddies of the California Current System offshore, which blocked or steered the cold upwelled water. The space and time scales of the mesoscale variability were much shorter than have been previously observed in deep-water eddies offshore. Additional process studies are needed to elucidate the dynamics of the flow.

1. Introduction

The drive towards integrated coastal-ocean observing systems has fostered the need for basic research not only on the individual elements composing such systems but also on how to make these elements function together smoothly as a whole. As a step towards providing improved coastal forecasting over the coming decades, the second Autonomous Ocean Sampling Network (AOSN-II) experiment was conducted in the Monterey Bay during late July–early September 2003. The objective of the Predictive Skill Experiment was to learn how to apply new tools, technologies, and analysis techniques to adaptively sample the coastal ocean in a manner demonstrably superior to traditional methodologies, and to use the information gathered to improve predictive skill for quantities of interest to end-users. These quantities might include the location of fronts and boundaries relevant to outfall dispersal, particle trajectories for people or pollutants in the water, and the biological response to ocean

* Corresponding author.
E-mail address: sramp@mbari.org (S.R. Ramp).

0967-0645/$ - see front matter © 2008 Elsevier Ltd. All rights reserved.
doi:10.1016/j.dsr2.2008.08.013

physics in the form of bioluminescence or harmful algal blooms. The goal necessitates an underwater, through-the-air, and over-land networking infrastructure from which the program takes its name.

Although AOSN-II was a novel collaborative effort involving state-of-the-art autonomous observing platforms and two data-driven models running in real time (Chao et al., 2009; Haley et al., 2009) with data assimilation and ensemble uncertainty predictions (Lermusiaux, 2007), the AOSN-II project was influenced by previous real-time applications of observing networks and modeling systems in coastal regions. Some of the early ocean observing and prediction system (OOPS) efforts are reviewed by Robinson et al. (1998) and Robinson and Lermusiaux (2002). Significant observing and prediction coastal efforts also are described in manuscripts (Lynch and Davies, 1995; Mooers, 1999; Pinardi and Woods, 2002) and review articles (e.g., Robinson and Glenn, 1999; Dickey, 2003; Lermusiaux et al., 2006). Without being exhaustive, research on coastal OOPS include scientific research exercises in: Boston Harbor and Massachusetts Bay (Littoral Ocean Observing and Prediction Systems: Robinson and the LOOPS group, 1999; Lermusiaux, 2001); in Georges Bank (Lynch et al., 2001); and, in the Martha's Vineyard region within the Coupled Marine Boundary Layers and Air–Sea Interaction Initiative (CBLAST: Edson et al., 1999, 2006). AUVs and models also have been jointly utilized within sustained efforts in the Gulf of Maine such as the Gulf of Maine Ocean Observing System (GoMOOS, Bogden et al., 2001) and the Regional Association for Research on the Gulf of Maine (RARGOM: Runge, 2005). Several of these research activities in the Northeast involved coupled physical–biological observing and modeling research, from determining dominant scales to targeted process studies, e.g., Ecology of Harmful Algal Blooms/Global Ocean Ecosystem Dynamics (ECOHAB/GLOBEC: Anon., 2002, 2005; Wiebe et al., 2001) and LOOPS (Besiktepe et al., 2003), but for biological–physical data collection and modeling in real time, interesting challenges remain (e.g., deYoung et al., 2004). The first Long-term Ecosystem Observatory (LEO) research with advanced ocean and observing prediction systems has been maintained off the coast of New Jersey, with numerous data-model integrated coastal studies and results (e.g., Schofield et al., 2002; Wilkin et al., 2005). Important research has also being carried out in the Gulf or Mexico and its larger region of influence (Mooers et al., 2005). Numerous scientific results also have been obtained off the coast of Oregon as a result of coupled observation and modeling experiments (Barth and Wheeler, 2005). All of these research efforts are now better coordinated and developed at the national level, within programs such as the Integrated and Sustained Ocean Observing Systems (Ocean.US, 2002, 2004). At the international level, several exercises were sponsored in multiple regions by the North Atlantic Treaty Organization within the Rapid Environmental Assessments and Rapid Response exercises (Bovio et al., 2003; Robinson et al., 2003; Onken et al., 2002, 2005). Specifically, the first adaptive sampling based on real-time data-driven uncertainty predictions was carried out within in a NATO research exercise in the Strait of Sicily region (Robinson et al., 1999, Lermusiaux, 1999).

While many of the objectives of the AOSN-II experiment were practical in nature, the AOSN-II science team formulated a list of scientific goals as well including:

- Observe and predict the development and movement of upwelling fronts and ocean eddies.
- Determine the importance of the wind-stress curl in driving upwelling and the three-dimensional circulation in the Monterey Bay.
- Study the relationship between micro-scale atmospheric jets and the formation of oceanic cold plumes off coastal headlands and promontories.
- Examine the nutrient supply processes in the Monterey Bay including upwelling, advection, and mixing.
- Evaluate and improve numerical models of both the atmosphere and the coastal ocean.

The Monterey Bay provides an ideal location for such an experiment due to its close proximity to several large research institutions, ship availability, and the wealth of environments and scientific problems presented. The wide continental shelves within and to the north of the bay provide a strong contrast to the nearby deep water within the Monterey Bay Submarine Canyon (MSC) and the narrower, steeper shelf to the south. The two upwelling centers at Point Sur and Cape Año Nuevo are both within a day's steam by research vessel. Much of the communications infrastructure including undersea cables, semi-permanent moored surface buoys, and a wireless Internet network was already established by the Monterey Bay Aquarium Research Institute and various local Navy entities. A network of coastal HF radars was already in place monitoring the surface currents in real time. The installation of the additional elements required for the AOSN-II experiment to the existing observing system in the bay was straightforward.

The mesoscale variability near the Monterey Bay can be succinctly described as the interplay between the upwelling centers rooted at headlands to the north and south of the bay and a persistent, anti-cyclonic California Current meander just offshore of the bay itself (Ramp et al., 2005). The upwelling centers are clearly driven by the prevailing northwesterly winds, which are strongest during March–June (Nelson, 1977). The flow off Año Nuevo is sometimes bifurcated (Rosenfeld et al., 1994), with some of the cold, salty upwelled water flowing offshore and some flowing south over the Monterey Canyon. This pattern seems to depend on the wind-stress duration: The cold water spreads southward only after a strong, steady northwesterly wind has been blowing for about 6–7 days (Ramp et al., 2005).

To the south of the bay, a strong upwelling center located at Point Sur generates cold filaments moving offshore in the upper 100 m (Breaker and Mooers, 1986; Tisch et al., 1992; Rosenfeld et al., 1994; Ramp et al., 1997). On the continental shelf there, currents were equatorward during northwesterly winds and poleward during wind reversals and relaxations (Ramp and Abbott, 1998). These authors found that the vertical structure of equatorward currents was consistent with the superposition of the local wind-forced Ekman spiral and the alongshore geostrophic flow due to the set-down at the coast. The poleward flows during relaxations were dynamically consistent with a poleward alongshore pressure gradient force, as observed at other locations off California (Winant et al., 1987; Lentz, 1987). These currents are consistent with the view that cold surface water in the center of the Monterey Bay is advected from the north of the bay and not the south.

The anti-cyclonic California Current (CC) meander, also sometimes referred to as the Monterey Bay Eddy (MBE), is a frequently observed feature of the region during the upwelling season (Rosenfeld et al., 1994; Paduan and Rosenfeld, 1996; Ramp et al., 2005). Drifters suggest that this feature is associated with the larger-scale, meandering California Current System and is not locally generated (Brink et al., 1991). Moored observations show that the feature is deep, with coherent flows greater than 20 cm/s exceeding 1000 m depth (Ramp et al., 1997). The feature is warm and fresh relative to the local waters, displaying the influence of the Pacific Subarctic Water (Rosenfeld et al., 1994). The MBE is

thus an oceanic feature and is clearly not generated by the local wind stress, although it does respond to it. Time series of sea-surface temperature from aircraft and AVHRR images show that the MBE moves rapidly onshore during wind relaxation events and retreats back offshore when the winds reintensify (Rosenfeld et al., 1994). Moored observations, however, also have shown an onshore and southward translation of the MBE without a wind relaxation (Ramp et al., 1997). The mechanism for this across-shore eddy translation is thus not fully understood.

Coursing poleward beneath the upwelling centers and CC meander lies the sub-surface California Undercurrent (CUC). The CUC is observed over the continental slope all along the west coast of the United States (Pierce et al., 2000) and is a ubiquitous feature of all moored data sets both north and south of the Monterey Bay. To the north off the Farallon Islands, the undercurrent was present most of the year but was not coherent with local wind forcing (Noble and Ramp, 2000). To the south off Point Sur, the currents below 100 m depth are more often poleward than equatorward and frequently exceed 30 cm/s at 100 m (Chelton, 1984; Wickham et al., 1987; Tisch et al., 1992; Ramp et al., 1997). The poleward flow off Point Sur is pulse-like at very low frequencies (3–4 months) (Ramp et al., 1997). How this pulse-like flow relates to cross-shore translations of the MBE and potential "blocking" of the CUC by the eddy is of interest but poorly understood.

The circulation in the bay itself is usually cyclonic (Paduan and Rosenfeld, 1996; Paduan and Cook, 1997; Ramp et al., 2005) during both upwelling and downwelling conditions. During upwelling events, very warm ($>16\,^{\circ}$C) water is observed in the northeast corner of the bay, in the wind shadow behind the Santa Cruz mountains (Graham, 1993; Graham and Largier, 1997; Ramp et al., 2005). Model salinity fields at the surface and 100-m levels show that the bay fills with higher-salinity water stemming from the Point Año Nuevo upwelling center under these conditions. During downwelling, the cyclonic circulation was more barotropic over the continental shelf than during upwelling events. The source water for both the surface and 100-m levels was the colder, fresher California Current water offshore, which had advected southward well past Point Pinos during the previous upwelling event and entered the bay from the south (Ramp et al., 2005)

2. Data and methods

An impressive array of sampling platforms was assembled for AOSN-II including ships, aircraft, gliders, and propeller-driven AUVs, with each deployed to optimize its sampling strengths (Fig. 1). Gliders are buoyancy-driven vehicles that are slow but can remain deployed for several months at a time (Bellingham et al., 2009). Propeller-driven vehicles can sustain speeds of 6 knots but only for 14 h or less per deployment. Ships collect the highest-accuracy data and can collect water from throughout the water column for chemical analyses. Aircraft can obtain a "snapshot" of the sea-surface conditions in 5 h or less, but with less accuracy than ships.

Five Spray gliders (Sherman et al., 2001; Davis et al., 2002) were deployed during AOSN-II from July 23 to August 24, 2003 along 5 linear tracks covering from Point Año Nuevo in the north to Point Sur in the south, out to roughly 100 km offshore (Fig. 1). Beyond instrument development and testing operational capabilities, the goal for these gliders was to contribute data for

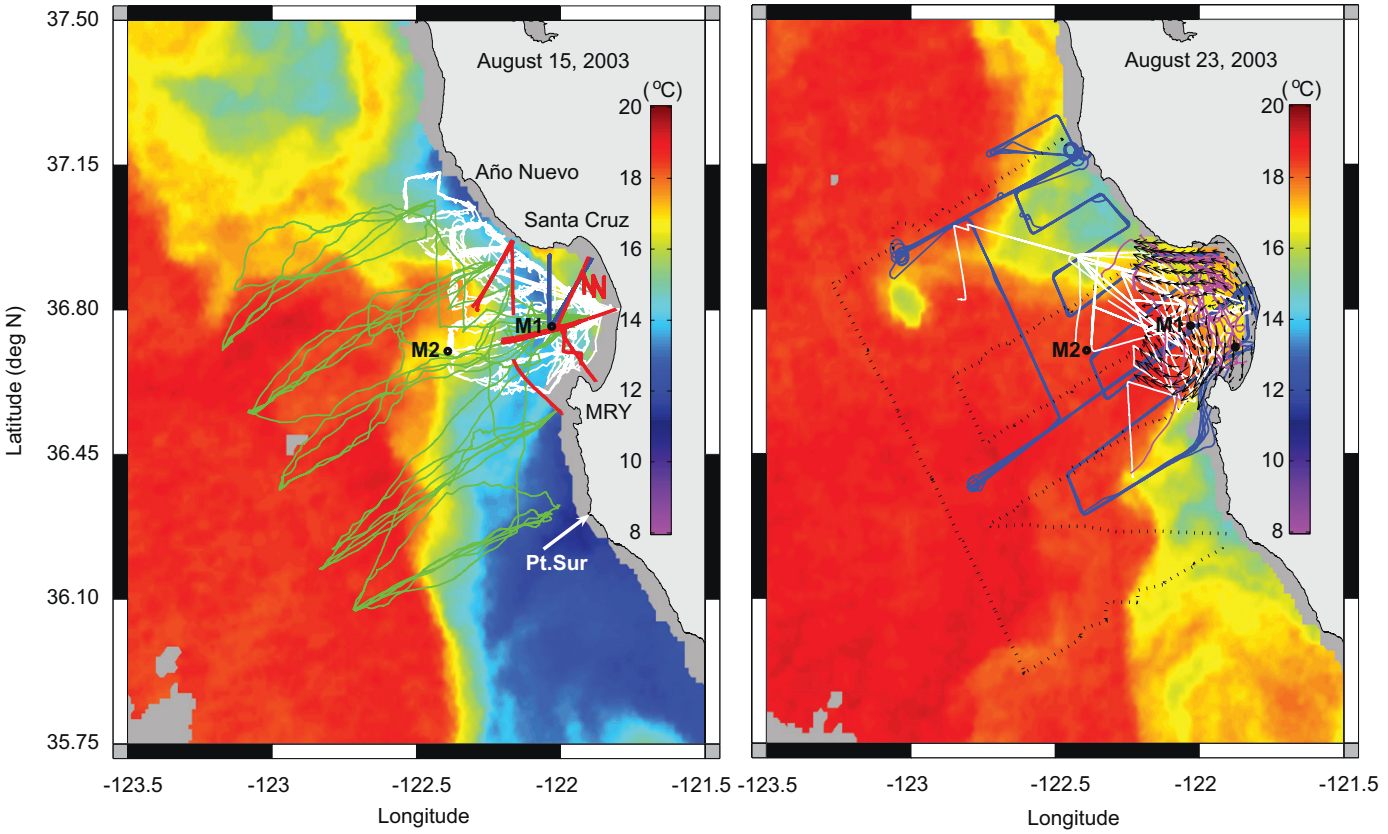

Fig. 1. Sampling locations for autonomous vehicles (left) and other assets such as ships, aircraft, and HF radars (right) during AOSN-II. Green tracks were obtained from the Spray vehicles and the white tracks from the Slocums. The blue "V" track was occupied at night by the CalPoly REMUS vehicle. The other red tracks were occupied by the MBARI DORADO vehicle and the NPS REMUS vehicle. The dark blue track on the right is the aircraft flight path, and the thin dotted line with station locations is the POINT SUR ship survey. The vectors in the Monterey Bay are the surface currents as sensed by coastal HF radars. Both sampling schemes are overlaid on satellite AVHRR sea surface temperature (SST), as indicated by the color bar.

assimilation and synoptic mapping and to define the scales and patterns of variability. These gliders collected a total of 2075 vertical profiles to 400 m depth (or the bottom) with a nominal spatial resolution of 2.3 km. The resolution is a function of bottom depth and higher resolution was obtained in shallower water. In addition to temperature, salinity, and water clarity, each glider also returned an estimate of the vertically averaged horizontal current during each profile, obtained as the difference between actual GPS position and dead reckoning. A Spray glider can typically make only about 22–25 cm/s of forward progress through the water, which necessitated the across-shore racetracks to avoid fighting the primarily alongshore current in the region. It took each glider nominally 4 days to transit one way along each 100-km racetrack.

Overall Spray glider performance was excellent during AOSN-II. The gliders, once deployed, required no servicing and lasted for the duration of the experiment on one set of batteries. The limiting factor on good data collection turned out to be biofouling rather than battery life. For additional details, see the accompanying technical article (Bellingham et al., 2009).

Ten Slocum gliders profiled to 200 m depth, and were thus deployed closer to shore than the Sprays (Fig. 1). Four Slocum gliders ran closed boxes (or "cells") rather than linear tracks, and were equipped with fluorescence and photosynthetically available radiation (PAR) sensors in addition to the variables sensed by the Spray. A total of 11,341 profiles yielding nominally 800 m along-track resolution were obtained over the life of the experiment. The endurance of the Slocums was 11–14 days, about half that expected, and some recovery and re-deployment was thus required to cover the lifetime of the experiment. The Slocums also experience problems with biofouling, but the shorter deployments allowed for cleaning of the sensors to minimize this problem.

One of the most innovative aspects of the AOSN-II experiment was adaptive sampling of ocean features using gliders (Leonard et al., 2007). Three to four Slocum gliders were used for this purpose. Three demonstrations of autonomous adaptive control were successfully completed, one in the northern part of the bay across an upwelling front, the second in the southern part of the bay, and the third following a surface drifter (Fiorelli et al., 2006). For the first experiment during August 6–7, 2003, three gliders maintained a triangular pattern 3 km on a side while propagating NW along a linear path. The triangular formation was chosen so that in-situ estimates of gradients (e.g., in temperature) along the path of the center of the formation could be computed in near-real time from the gliders' scalar (temperature) measurements. The gliders could be programmed to follow the gradient if desired. The 3-km sensing array resolution was designed with respect to previously computed scales in Monterey Bay. The formation error was 423 m, or 14% of the desired spacing with a standard deviation of 159 m. For the second demonstration on August 16–17, 2003, some additional difficulty was added. The triangle formation was asked to travel a zigzag path across an upwelling front, and to shrink the size of the formation from 6 to 3 km on a side enroute. The objective was to demonstrate the ability of the glider control system to adjust the formation size, i.e., the sensing array resolution, in response to changing scales in the sampled field(s) and to provide gradient estimates at different resolutions. This exercise was also a success: The glider formation error was a function of the size of the triangle, about 394 m for the 6-km triangle and 270 m for the 3 km one. Finally, on August 23, 2003, a single glider was asked to follow a surface drifter in real time, making zigzags across its projected path. The goal was to demonstrate that a glider or glider formation could collect scalar measurements (or gradient estimates) both across and below tracer paths. This demo was qualitatively a success, but there were some problems based on the different velocity fields sensed by the two instruments: The drifter measures the surface velocity while the glider measures the current vertically integrated over the up/down path, making coincident path prediction difficult. There are other (easier) ways to do this, such as having the glider follow the drifter with a two-hour lag, which may be more useful in different applications.

Propeller-driven AUVs such as the commercially available REMUS, the MBARI manufactured DORADO, and the NPS in-house vehicle ARIES typically have about 14 h duration at 4–6 knots. The vehicles also have a much larger payload than gliders and can thus carry more sophisticated sensors. The largest number of transects were run by the California Polytechnic State University (CalPoly) REMUS vehicle along two transects in the northern half of the Monterey Bay. The goal of sensing bioluminescence dictated that these REMUS runs be done in the dark, and therefore 9 seven-hour missions were completed along 45 km transects between 9 pm and 4 am each night (blue "V" in Fig. 1). These operations began near Santa Cruz, ran out to MBARI surface buoy M1, then returned to the NW corner of the bay (Moline et al., 2005; Shulman et al., 2005). The vehicle followed a saw-tooth pattern to 40 m depth sampling with a CTD, transmissometer, fluorometer, and ADCP in addition to the bioluminescence. Four transects were also run from Monterey to M1 using the NPS REMUS vehicle, sampling temperature only. The NPS ARIES vehicle was used exclusively to fetch data from a bottom-mounted ADCP using acoustic modems and did not collect environmental data.

The largest AUV used during AOSN-II was the MBARI DORADO AUV. This vehicle ran along a line between Moss Landing and MBARI buoy M2, profiling to 250 m depth (Fig. 1). Instruments on board included a CTD, fluorometer, oxygen and nitrate sensors, bioluminescence, and ADCP. The run was made operationally every 3 weeks, but the frequency was increased during August 2003 to 1 section per week. Two additional DORADO transects also were conducted offshore. A clear advantage of this vehicle was the sampling depth, which was very helpful for model data assimilation. Its large size requires a specialized vehicle for recovery.

The airborne measurements during AOSN-II were obtained using the TWIN OTTER aircraft owned and operated by the Center for Interdisciplinary Remotely Piloted Aircraft Studies (CIRPAS) at the Naval Postgraduate School. Fourteen flights were conducted between August 4 and September 5, 2003 at an altitude of nominally 33 m above the sea surface. The low altitude was chosen to pass beneath the stratus cloud deck that often covers the Monterey Bay in summer, and to minimize the vertical divergence in the heat and momentum flux observations. The flight path (Fig. 1, blue line) covered all of the bay and some distance to the north and south out to 100 km offshore. Two vertical saw-tooth paths to 1500 m also were conducted along two slightly longer transects at the northern end of the flight path and along the center of the bay (Fig. 1). These paths were to sample the three-dimensional structure of the marine atmospheric boundary layer over the bay (Kalogiros et al., 2006; Wang et al., 2007). The atmospheric parameters sampled by the aircraft included air temperature and dew point, atmospheric pressure, wind speed and direction, the turbulent fluxes of heat and momentum, and total particle number, as well as aerosol and cloud/fog droplet size distributions. In the ocean, sea-surface temperature (SST), ocean-leaving radiance at 193 wavelengths, sun glint, and surface roughness were observed. The SST, air temperature and dew point, and wind data were made available for model assimilation in near-real time, while the other parameters required additional post-processing.

Coastal HF radars for mapping ocean surface currents have been proliferating along the central coast for a period of years,

starting with three standard-range (13 MHz) systems in the Monterey Bay located at Point Pinos, Moss Landing, and Santa Cruz. The network has recently been extended to the north with long-range (5 MHz) systems at Big Creek, Pescadero, and Montara. All the bay systems were operational during AOSN-II and provided surface currents in 2–3 km bins for model data assimilation (Paduan and Shulman, 2004; Shulman and Paduan, 2009) and Lagrangian Coherent Structures (LCS) computations.

3. The numerical models

A key aspect of AOSN-II program was to assimilate the data collected in near-real time into mesoscale ocean models to forecast conditions for the following day, and adapt the sampling scheme accordingly. In addition to real-time operations, the models also were used to help elucidate the dynamics of the flow. Three models were used for these purposes, namely the Harvard Ocean Prediction System (HOPS) (Robinson, 1999), the Jet Propulsion Laboratory implementation of the Regional Ocean Modeling System (JPL/ROMS) (Shchepetkin and McWilliams, 2004), and the Navy Coastal Ocean Model/Innovative Coastal Ocean Observing Network (NCOM/ICON) (Shulman et al., 2002, 2004). While conceptually similar in scale (1.5–2.5 km in the horizontal $\times$ 32 sigma levels in the vertical) and operation, the models differed significantly in terms of the mixing schemes employed, initial conditions used, spin-up time, and open-boundary conditions provided by the larger-scale models they were nested within. All three models were forced using the Coupled Air Ocean Modeling and Prediction System (COAMPS^{TM}) surface wind stresses and heat fluxes, and assimilated the aircraft SST, glider T and S, and AUV data. The JPL/ROMS model additionally assimilated T and S data from MBARI moorings M1 and M2. None of the models assimilated velocity from moorings or HF radar. A table with additional details of the three models, the data assimilation schemes used, and how they were forced may be found on the web at: (http://www.princeton.edu/~dcsl/asap/ASAP_ROMS_HOPS_NCOMICON_summary_MB06.doc).

4. Results

4.1. Atmospheric forcing

The weather presented an interesting mix of conditions that were well suited to the experimental objectives during August 2003. Time series from MBARI buoy M2, located at 36°42′N, 122°23′W at the mouth of the bay, show that the first two flights during August 4–5 took place during a wind relaxation event when winds were weakly poleward at less than 5 m/s (Fig. 2). An extended period of strong (commonly 10 m/s), steady, upwelling-favorable northwesterly winds followed during August 6–19, which were quite typical for this time of year. Five TWIN OTTER flights sampled this first upwelling event. Another poleward event took place during August 20–21, followed by a second upwelling event from August 23–31. Three flights were executed during the relaxation and two during the second upwelling event. September 1–3 was very calm and warm in the Monterey Bay and was characterized by nearly flat seas and strong surface heating. This time period was unfortunately not sampled by the aircraft. During

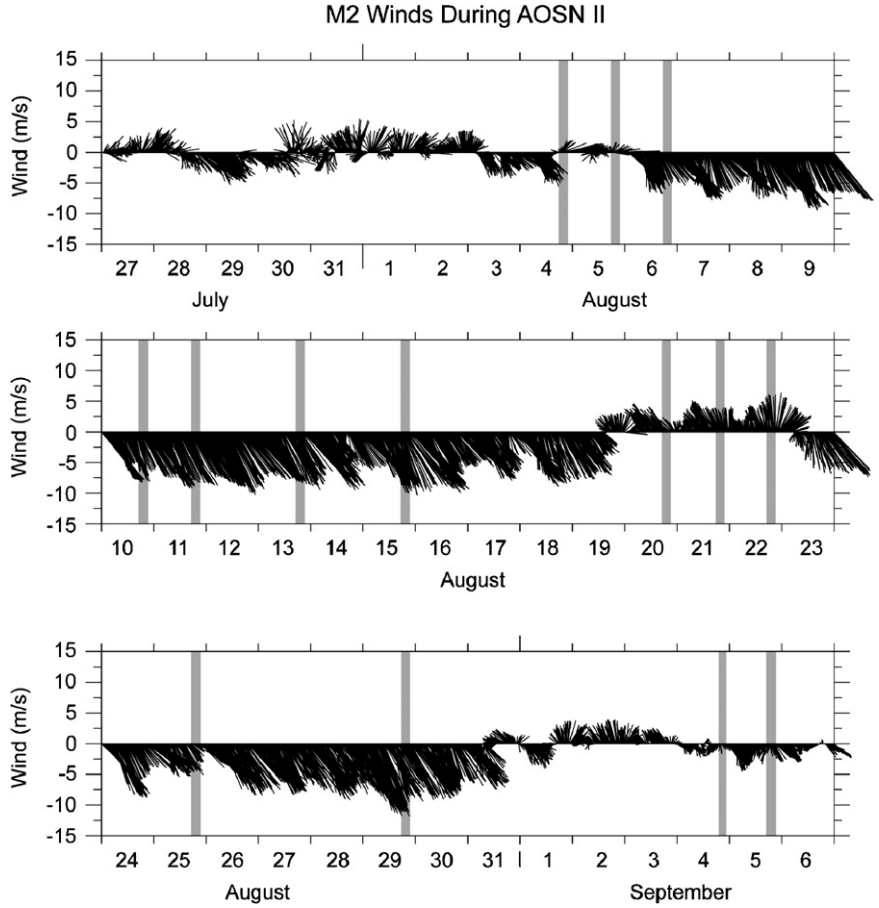

Fig. 2. Low-pass filtered surface wind vectors from Buoy M2, located at 36°42′N, 122°23′W, maintained and operated by the Monterey Bay Aquarium Research Institute (MBARI). The gray vertical bars indicate the time of the NPS TWIN OTTER aircraft over-flights.

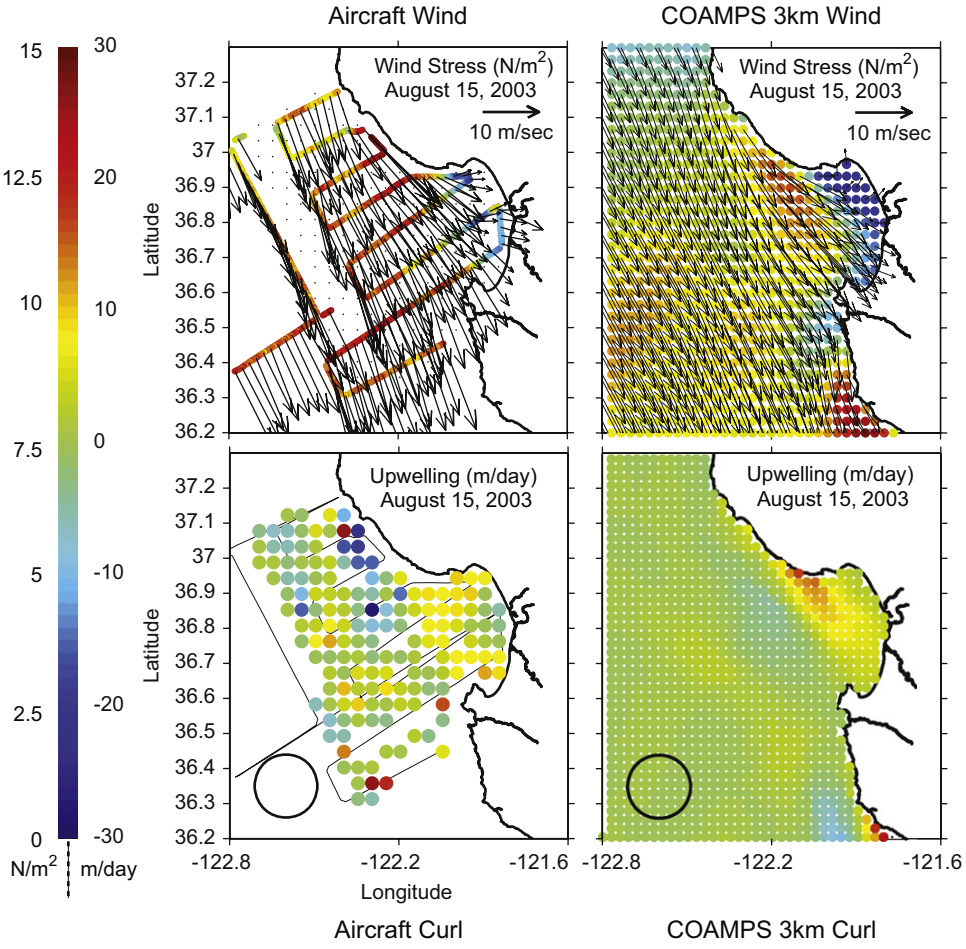

Fig. 3. A comparison of the wind, wind stress, and the wind-stress curl between the observed values sampled by the aircraft and the output from the 3-km COAMPS™ model on August 15, 2003 during an upwelling event. Common scales have been adopted for both pictures. The wind speed displayed as vectors are overlaid on the color-coded wind stress as indicated by the left side of the color bar. The wind-stress curl translated into upwelling velocities in m/d are indicated by the lower panel dots and the right-hand scale of the color bar. The black circle in the lower panels indicates the size of the domain used to compute the curl of the wind stress.

September 4–6, weakly upwelling-favorable winds returned to the area once again, and the final two aircraft over-flights were conducted.

Since the spatial scales of the atmospheric forcing are large compared to the size of the Monterey Bay (22×40 km), the winds observed at buoy M2 are usually representative of the offshore winds elsewhere along the coast (Fig. 3). Within the bay itself, however, the surrounding mountains create high spatial variability in the surface wind stress. Of particular interest are the weak winds behind the mountains in the NE corner of the bay, and a small-scale atmospheric jet coming through a gap in the mountains off Santa Cruz (Fig. 3). This figure from August 15 was sampled 9 days into the upwelling event and was typical of the others during this time. The aircraft and the Coupled Ocean–Atmosphere Mesoscale Prediction System (COAMPS) (Doyle et al., 2009) both show the upwelling-favorable winds turning slightly into the bay. Both also show the weak (blue) winds in the NE corner of the bay. The wind jet off Santa Cruz was slightly clearer in the model output than the observational data, as was the strong positive curl on the inshore side of the jet (Fig. 3, bottom). The location and scale of this feature closely resembled a similar one observed on August 17, 2000 (Ramp et al., 2005). While that jet was noticeably hot and dry (their Fig. 4) this was less obvious in the 2003 data. This is perhaps due to the higher altitude (133 m) of the year 2000 flights. The 2003 atmospheric temperatures at 33 m (not shown) more closely followed the sea-surface temperature and were cool rather than warm. There was a minimum in the dew point temperature just off Santa Cruz, however, indicating slightly dryer conditions there. A typical poleward wind event from August 20, 2003 (Fig. 4) showed overall weaker winds, weaker gradients, and less wind-stress curl than a typical equatorward wind event. The wind stress was still weaker in the NE corner of the bay than elsewhere, and the wind turned into the bay from the south rather than the north.

4.2. Development and relaxation of the upwelling plume

A time series of 12 realizations of SST and wind as sampled by the aircraft shows the ocean's mesoscale response to the equatorward and poleward wind-stress events during summer 2003 (Fig. 5A–L). August 4 was the first day of a relaxation event following a weak, 2-day upwelling event. The winds were weak and disorganized and some traces of coastal upwelling were still visible (<14 °C) off Point Año Nuevo. The warmest water exceeded 17 °C offshore and in the southern portion of the Monterey Bay. By the following afternoon (Fig. 5B), the entire sea surface had warmed by about 2 °C under weak, slightly onshore winds, with the exception of off Point Sur where the SST remained about the same. There was some indication of locally upwelling-favorable winds off Point Sur, which perhaps balanced the local surface heating.

The next five panels (Fig. 5C–G) show the development of the largest upwelling event. The August 6 image was obtained on

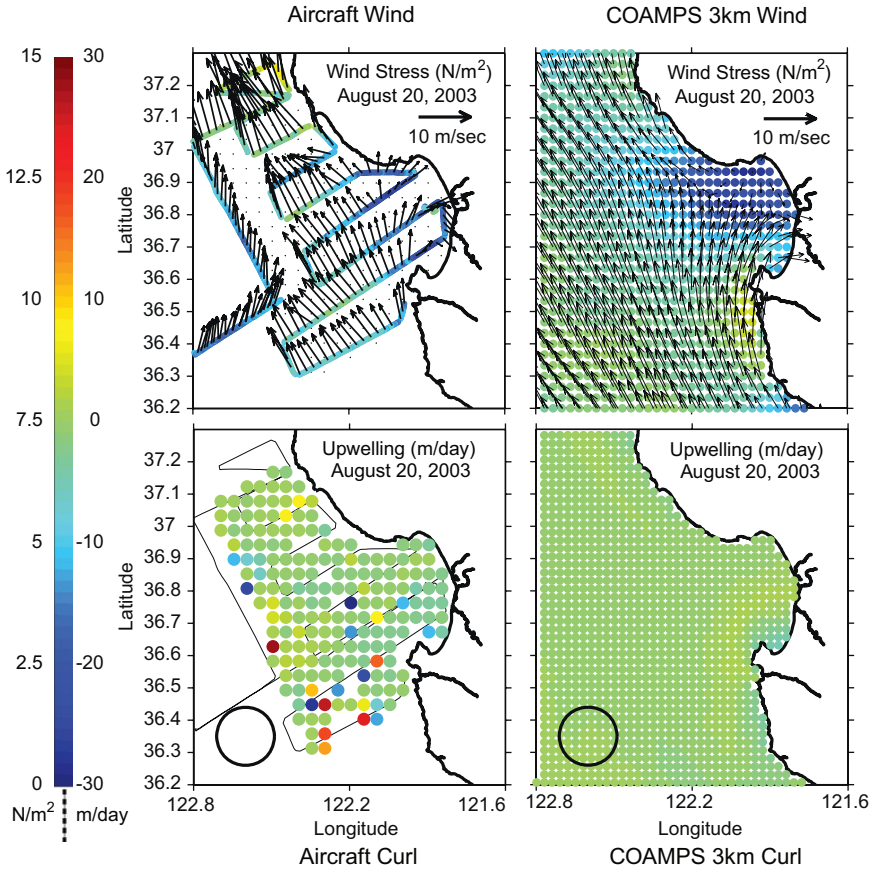

Fig. 4. As in Fig. 3 except on August 20, 2003 during a relaxation event.

the first day of strong (10 m/s) upwelling-favorable winds. The upwelling was just starting (yellow contour $<15\,^{\circ}$) at both Point Año Nuevo and Point Sur. Note that the aircraft survey was designed to focus on the Año Nuevo region and most of the Point Sur upwelling plume was located to the south of the flight path and was not observed. The discussion hereafter focuses on the growth and spreading of the Año Nuevo plume. Four days later (Fig. 5D) the upwelling center had enlarged and cooled considerably to less than 13 °C. There was some evidence of plume bifurcation (Rosenfeld et al., 1994) with some of the 14 °C water heading offshore and some heading south. By the next day however (Fig. 5E), southward advection seemed to be winning with all the 13 and 14 °C water heading south and connecting up with the cold water from the Point Sur upwelling center. This lead to a detached parcel of 13 °C water, which advected south on August 13 (Fig. 5F). Note that the CC meander, as indicated by the 17 °C contour, remained well offshore during this entire event, which allowed the cold water to follow an unobstructed path towards the south. On August 15, following 9 days of continuous upwelling, the winds were blowing at 15 m/s and the coldest water ($<12\,^{\circ}$C) was observed off both Año Nuevo and Point Sur. The cold water from the two centers merged together and formed a continuous band of minimum SST roughly along 122°06′W that separated the warm water offshore from the also warm water in the Monterey Bay.

The 2-week upwelling event was followed by 3 days of poleward winds at about 8 m/s on August 20–22 (Figs. 2 and 5H–J). The ocean's adjustment to the change in surface forcing was remarkably rapid and shows two noteworthy features (Fig. 5H). First, the boundary between the warm California Current water moved onshore to within just a few kilometers of the coast near Davenport, just north of Santa Cruz, CA. This dramatically reduced the amount of cold water at the surface in the northern portion of the domain. Second, a cold "squirt" formed in the southern half of the domain, centered near Point Piños in Monterey. Since the wind generally reverses from south to north along the coast, we speculate that this feature resulted from convergence between poleward currents along the southern Big Sur coast and currents that were still equatorward to the north of this region. This feature was still observable as a lens of 15 °C water 55 km offshore on August 21 (Fig. 5I) but was ultimately pushed back onshore by the continuing incursion of CC water on the 22nd (Fig. 5J).

The final two panels of Fig. 5 show the return to upwelling conditions, as represented by two realizations on August 25 and 29 (Fig. 5K, L). The 25th was just 2 days into the event and not surprisingly resembles August 6, with weak upwelling and $<15\,^{\circ}$C water off Cape Año Nuevo. August 29, 6 days into the event with winds >15 m/s closely resembles August 15. One significant difference would be that the CC was closer to shore on the 29th than the 15th, which confined the cold water closer to shore and resulted in strictly southward rather than offshore spreading. These differences in the two upwelling events were also evident in the output from the NCOM/ICON model (Fig. 6). The NCOM–ICON model is based on the Navy Coastal Ocean Model, and is triply nested inside of the global and regional (California Current) NCOM-based models (Shulman et al., 2004). The model is called NCOM ICON due to the fact that initial development of the model started under the National Oceanic Partnership Program (NOPP) Innovative Coastal-Ocean Observing Network (ICON) project (Ramp et al., 2005; Shulman et al., 2005). The top and bottom panels of Fig. 6 are a remarkably good match for Fig. 5G and L and show a more pronounced plume of cold, salty water moving offshore off Año Nuevo during the August 15 event than during

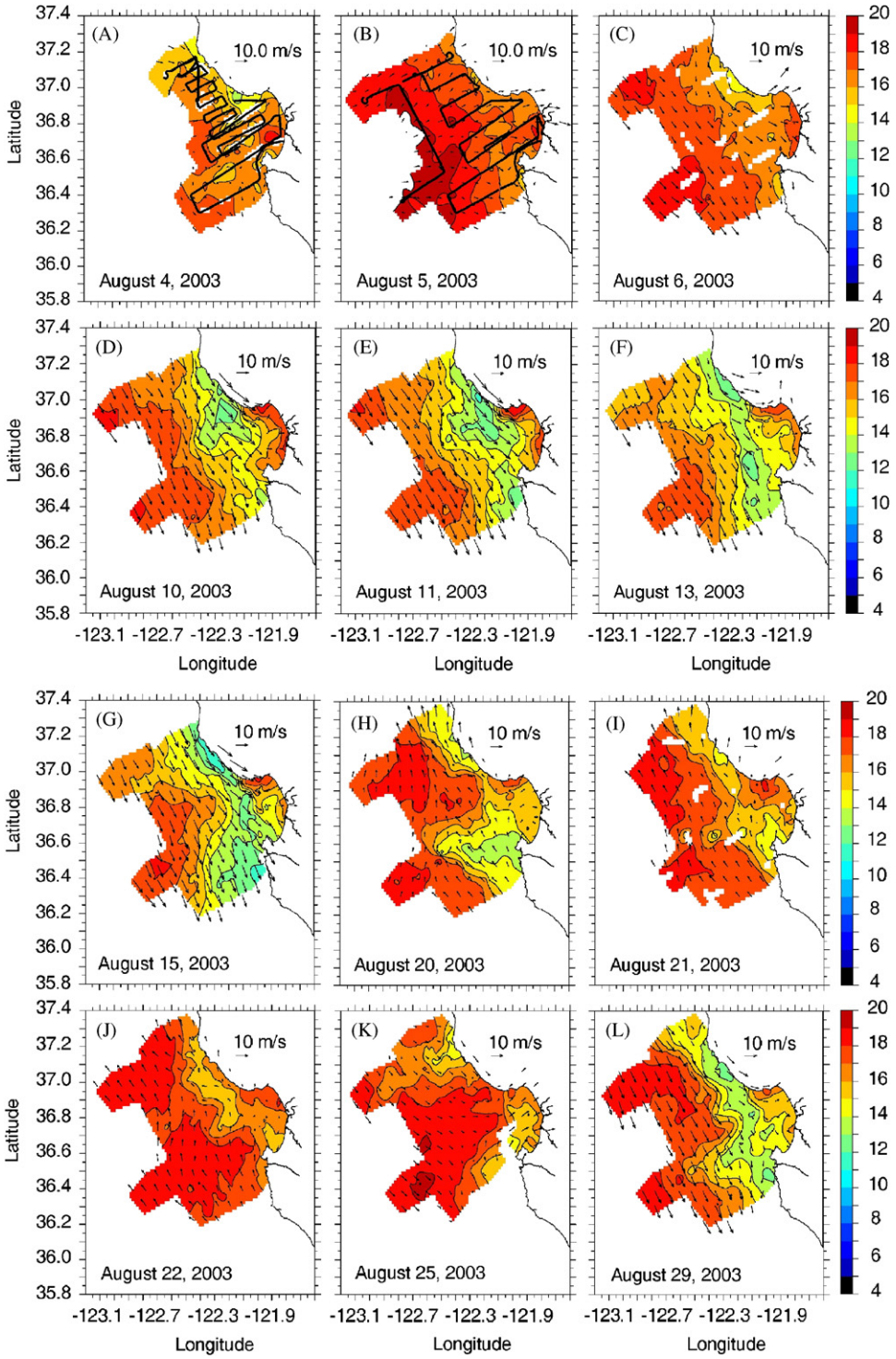

Fig. 5. (A–F) Time series of sea-surface temperature (SST, °C) and surface winds (m/s) as sensed from the aircraft during August 4–13, 2003. The flight path is indicated by the heavy black lines in panels A and B and the arrows indicate the magnitude and direction of the wind speed. (G–L) As in Fig. 5(A–F) except for August 15–September 4, 2003.

the August 29 event. The model fields show the Monterey Bay eddy to be much closer to shore during the latter event, centered near 36.6°N, 122.5°W with poleward flow on the offshore side. These eddy circulations were responsible for the offshore advection of the cold, salty plumes off Point Pinos and Point Sur, and for suppressing the offshore flow off Point Año Nuevo on August 29.

While the previous discussion focuses on the evolution of sea-surface temperature, some insight into the vertical structure of the evolving upwelling plume was also obtained from the glider formation flying experiments (GFFEs) described earlier. The first GFFE on August 6–7 sampled the front when it was young and close to the source at Point Año Nuevo and the second GFFE on August 16 sampled the front when it was older and had advected further to the south across the mouth of the Monterey Bay. In response to the strong upwelling-favorable winds measured on August 6 (Fig. 5C), three gliders were directed that same day to travel northwest, in an equilateral triangle with 3 km length sides, towards the Point Año Nuevo region to sample along the southwest side of the upwelling front (Fig. 7). Note that this formation flew against the prevailing current as sampled by

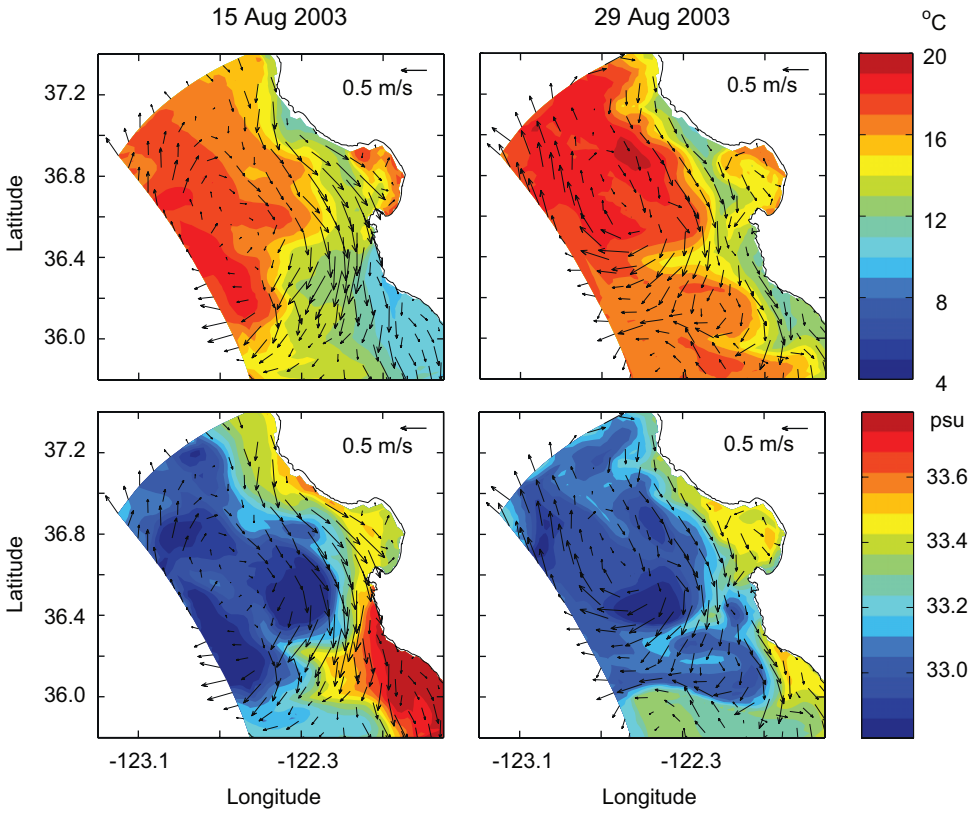

Fig. 6. Surface temperature (top panels), salinity (lower panels), and current vectors from the NCOM/ICON model for August 15 (left panels) and August 29, 2003 (right panels).

all the gliders (blue arrows in the figure), which would not be possible using conventional profiling floats or drifters. The temperature gradient estimate along the path provides a higher resolution complement to the SST (Fig. 5C) and in the corresponding AVHRR plots (not shown). The temperature gradients had the same sign at both depths shown (5 and 30 m), with warmer water offshore and approximately 1 °C cooler water inshore. The gradient was slightly stronger at 30 m, below the surface-mixed layer where spatial homogeneity tends to weaken the horizontal gradients.

During the second GFFE on August 16–17 the gliders traveled from near the center of the bay towards the southeast for about 12 h and then turned east and then northeast for a few more hours (Fig. 8). In this case the gliders moved mostly with the prevailing current (blue arrows) but also across and slightly against the flow towards the end. The temperature gradients in the horizontal plane were calculated from the glider-observed temperatures at 5 and 30 m depth along the path as in the August 6 experiment. During the first 12 h the glider triangle was straddling the inshore boundary of the upwelling front, i.e., the band of minimum SST near 122°06′W (Fig. 5G). At 5 m depth, the glider(s) furthest offshore measured cool temperatures of 11.5–12 °C in the extended plume while the gliders to the northwest measured warmer temperatures around 13 °C (Fig. 8). At 30 m, the temperature was nearly uniform (10 °C, dark blue) over much of the glider formation path, but with a weak gradient towards the northwest, opposite the surface layer. This indicates that the upwelling filament was quite shallow, less than 30 m deep, after it had advected southward across the Monterey Bay. By 45 m depth (not shown) the temperature gradient was very small.

4.3. Offshore structure

A central AOSN-II issue is how well the observing array can describe mesoscale ocean structure over the region of interest. Data-assimilating models can be powerful tools for synthesizing the scattered and diverse AOSN-II observations into a coherent picture, but these models can only describe that range of phenomena that approximately obey the model equations at the resolution they are solved. Little is known about what observations are needed to support an accurate and coherent synthesis of mesoscale coastal structure or how these data should be statistically characterized for the assimilation process. The observing power of the AOSN-II array is described by data collected over two separate one-week periods under contrasting wind forcing (Figs. 9–11). In the first week the offshore sampling density was not yet very uniform since the gliders were just getting on their assigned tracks (Fig. 9A). During the second week some gliders were moved off their assigned tracks by currents (Fig. 9B).

Winds over the last week of July and through August 6 were weak and variable (Fig. 2). While the moorings provide time series, the other platforms provide instantaneous samples along tracks and it takes about a week for them to map out the region. Even without upwelling-favorable winds for a week or more, near-surface temperatures are 2 °C or more colder near the coast than 50–100 km offshore. The mean alongshore- and time-averaged across-shore temperature section for this time period (Fig. 10A) shows the near-surface temperature gradient in Fig. 9A to be associated with isotherm slopes (and isopycnal slopes not shown) in the upper 50–100 m that support geostrophic shear with equatorward currents increasing near the surface. Below this, the isotherm and isopycnal slopes are reversed, producing geostrophic shear with poleward flow increasing above 100 m.

Upwelling-favorable winds began August 6 and persisted through August 19 (Fig. 2). Compared with the preceding calm period, near-surface temperature cooled about 2 °C within 10 km of the coast as the surface layer was blown offshore (Fig. 9B). This is also evident in the up-warping of the isotherms within 40 km of

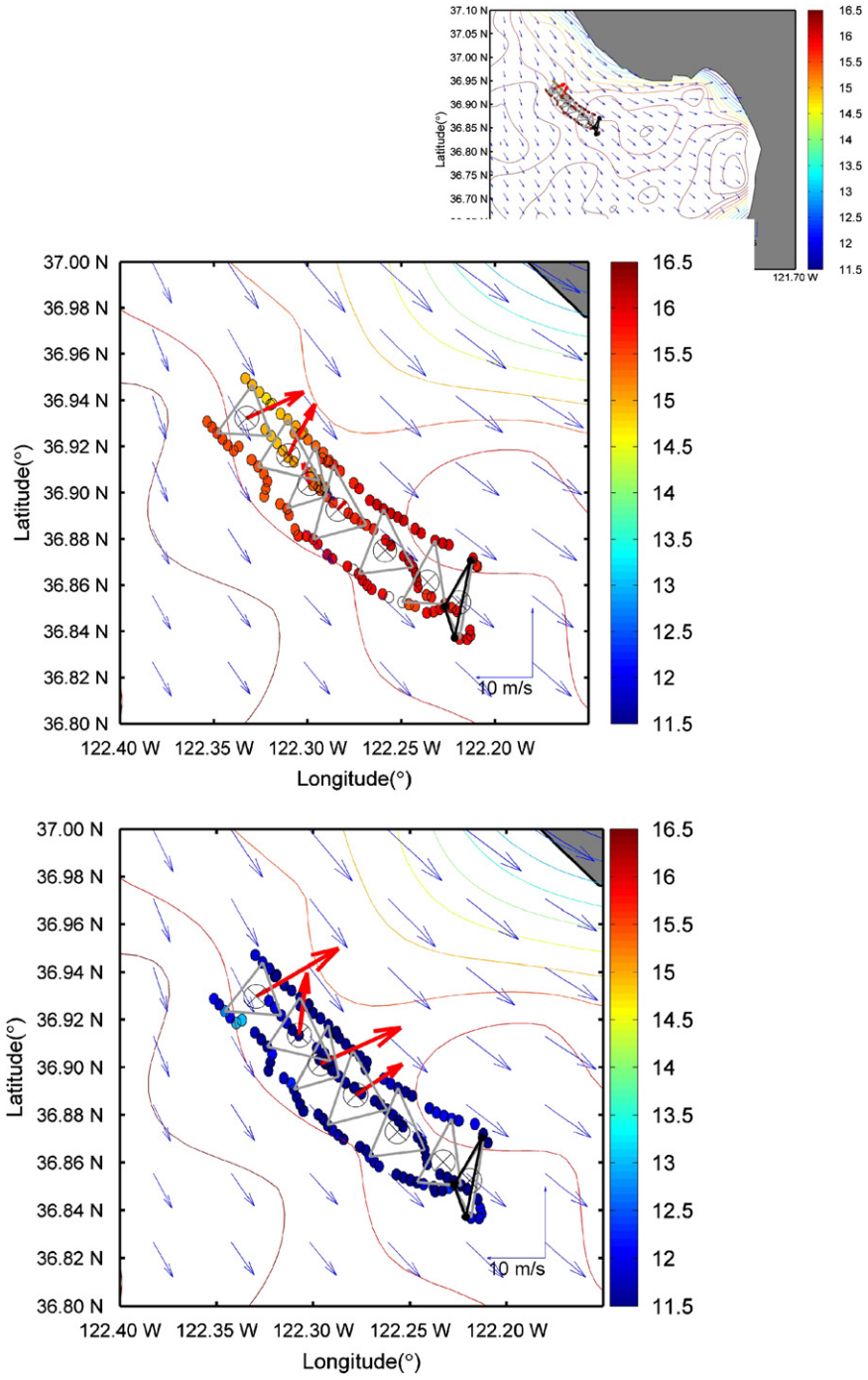

Fig. 7. Three gliders moving northwest in triangular formation (gray lines) from 18:00:00Z August 6 into late morning August 7, 2003. Colored dots indicate the temperature in °C at the 5 m (top) and 30 m (bottom) levels; black circles and lines show initial position and formation; and open circles with a cross inside triangles illustrate the path of the center of the triangle. Red arrows correspond to estimates of down-gradient temperature in the horizontal plane along the path of the center of the triangular formation. The color contours indicate SST as sampled by the TWIN OTTER aircraft. The blue arrows correspond to currents estimated with objective analysis using the gliders' depth-averaged current measurements.

the coast (Fig. 10B). In contrast, the temperature section shows that at distances of 50 km or more from shore the near-surface temperature increased up to 1 °C as a warm surface layer seems to have accumulated in a weakly stratified deep mixed layer (Fig. 10B). Below 100 m, no large-scale change in temperature or temperature gradient can be detected. The accumulation of warm water offshore under upwelling-favorable winds is surprising since there is no evidence that the wind strength or, consequently, the Ekman transport decreases offshore or that surface warming from above increases.

The offshore Spray gliders sample depth-averaged currents to 400 m and show a general, if structured, poleward flow offshore in both time periods (Fig. 9). This manifestation of the California Undercurrent was strongest during the weak-wind period when it took the form of a 20-km wide jet that meandered from 25 km offshore crossing the southernmost glider line to 65 km offshore on the northern line where it exhibited the strongest currents of nearly 30 cm/s (Fig. 9A). Equatorward wind in the second period significantly reduced the poleward signatures in depth-averaged velocity (Fig. 9B). Using depth- and alongshore-averaged current

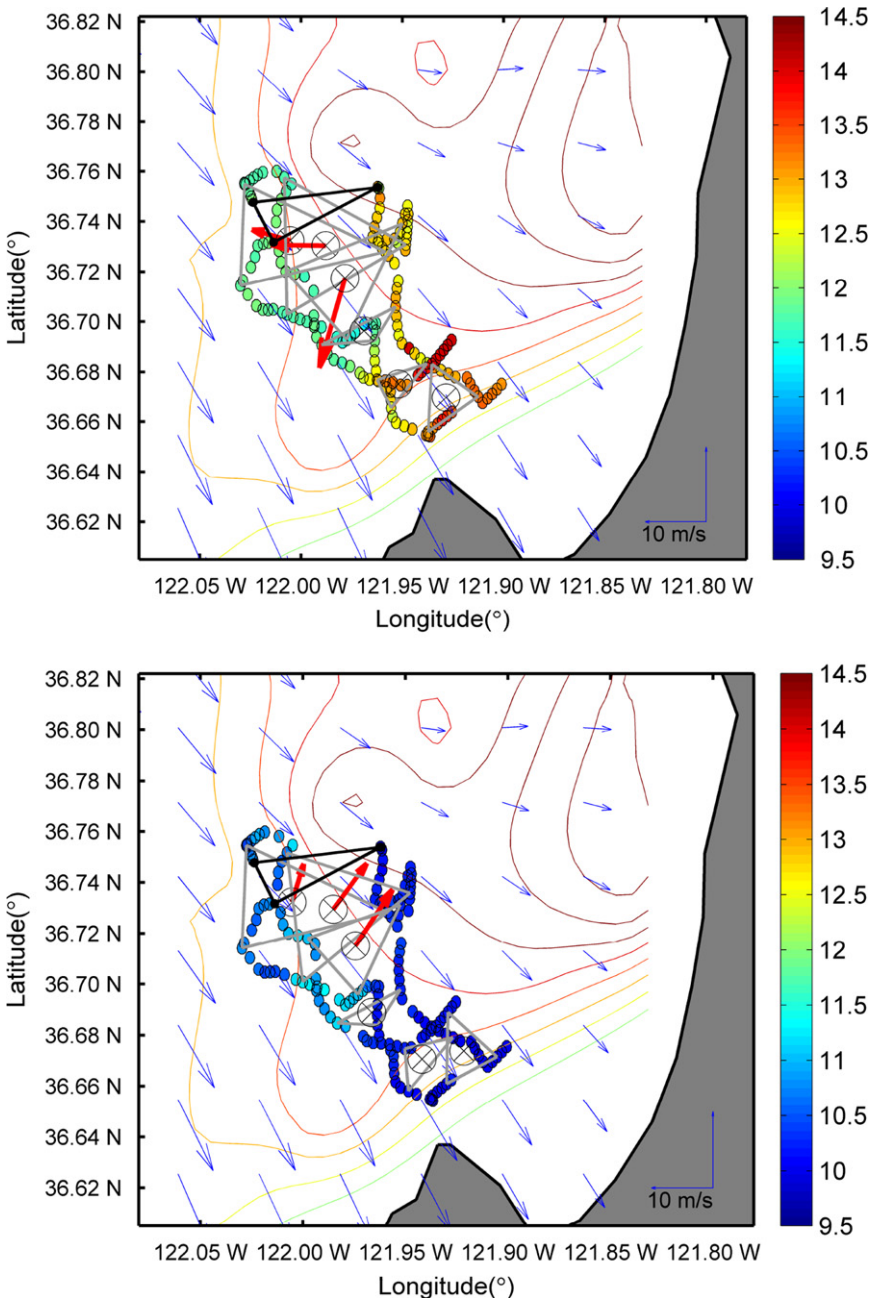

Fig. 8. Three gliders moving southeast in triangular formation (gray lines) during August 16–17, 2003. Colored dots indicate the temperature in °C at the 5 m (top) and 30 m (bottom) levels; black circles and lines show initial position and formation; and open circles with a cross inside triangles illustrate the path of the center of the triangle. Red arrows correspond to estimates of down-gradient temperature in the horizontal plane along the path of the center of the triangular formation. The color contours indicate SST as sampled by the TWIN OTTER aircraft. The blue arrows correspond to currents estimated with objective analysis using the gliders' depth averaged current measurements.

as a function of offshore distance to reference the alongshore geostrophic shear computed from alongshore- and time-averaged sections of temperature (Fig. 10) and salinity allows cross-sections of absolute alongshore velocity to be produced. These sections show that the decrease in poleward depth-average current from the first plotted week to the second resulted from offshore changes in geostrophic shear of alongshore current in the upper 150 m (Fig. 11). Also seen in Fig. 11 is how the equatorward upwelling jet in the second time period is largely confined to the 20 km closest to shore. More surprisingly, aside from these features, the general pattern of alongshore flow is moderately complex but remarkably similar between the two time periods even though no observation contributes to both time averages. It remains to be seen if this structure persisted for more than 16 days.

Beyond the alongshore- and time-averaged patterns described in Figs. 10 and 11, Fig. 9 shows complex and energetic smaller-scale features in both near-surface temperature and depth-integrated currents. Some of the complexity derives from plotting a full week of data together while other features may be a consequence of internal tides that are substantially aliased by shipboard and glider sampling. But some of the smaller-scale features have the appearance of eddies and fronts. Notable are oppositely rotating eddies found near the mouth of Monterey Bay. During the first week (Fig. 9A) the eddy is cyclonic with a clear poleward flow along the coast of Monterey Bay while it is

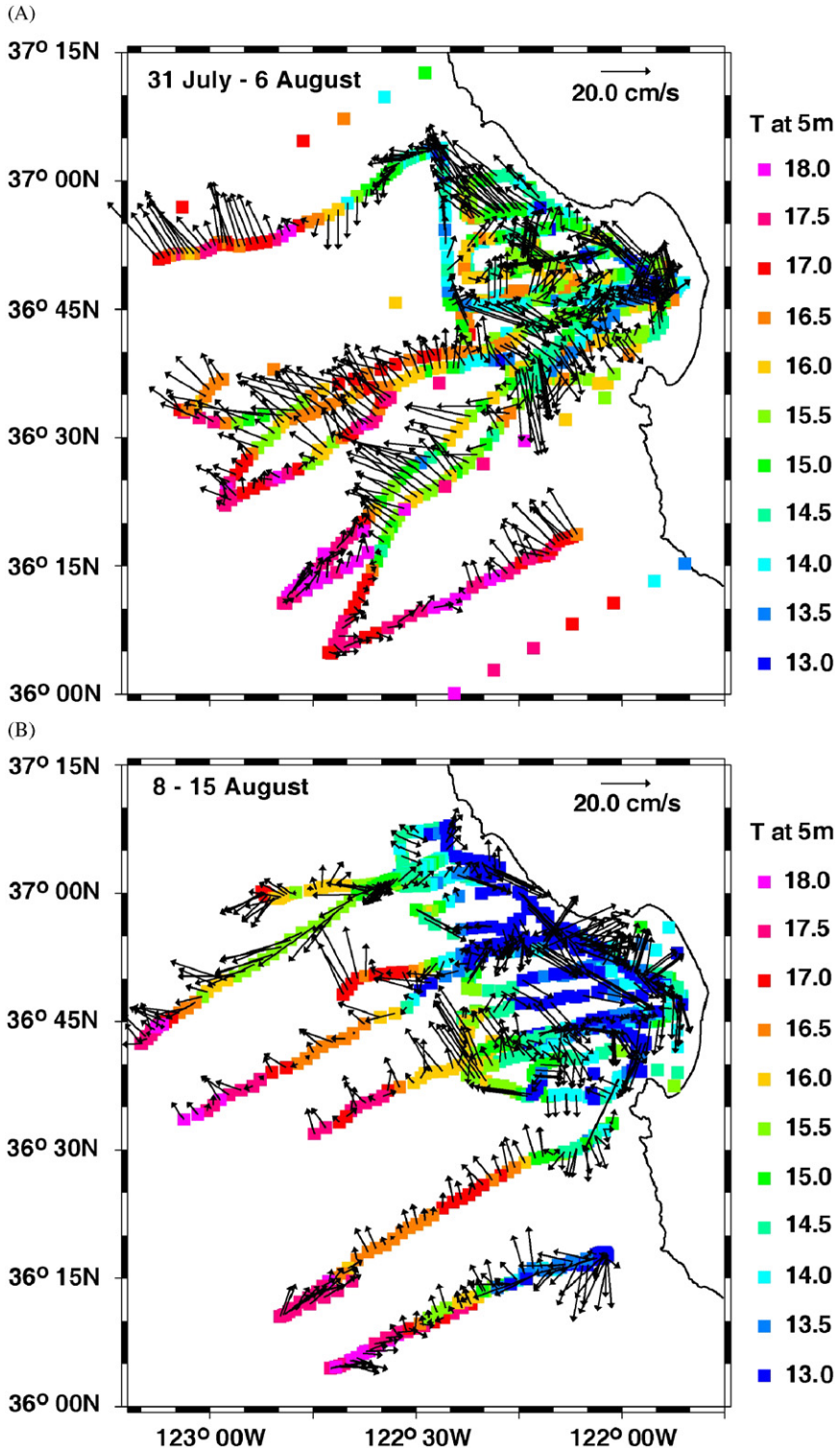

Fig. 9. Raw observations of 5-m temperature (colored squares, scale to the right) from AOSN-II ship surveys, moorings and gliders and depth-averaged velocity from gliders (black vectors, scale at upper right) from (A) July 31 to August 6, 2006 and (B) August 8–15, 2006. Spray gliders on lines extending well offshore sample to the bottom or 400 m while Slocum gliders on nearshore generally closed tracks sample to the bottom or 200 m.

anti-cyclonic in the August 8–15 upwelling period (Fig. 9B). The anti-cyclonic eddy is implicated as a cause of the spread of cold water away from Pt. Pinos (the southern end of the Bay mouth) seen in aircraft SST as shown in Fig. 5F–H spanning August 13–20.

The ability of the AOSN-II sampling array to describe the smaller-scale features hinted at in Fig. 9 depends on the spatial and temporal scales of those features. Roughly put, objective mapping (Bretherton et al., 1975) shows that mapping accuracy in the absence of assimilation into a dynamical model depends on the number of observations within sampling volumes whose dimension is set by the field's space and time scales. If there are enough points in each such volume to suppress small-scale noise the field can be mapped. In planning the AOSN-II field trial the scales of coastal variability were not well known. Fig. 12 shows the

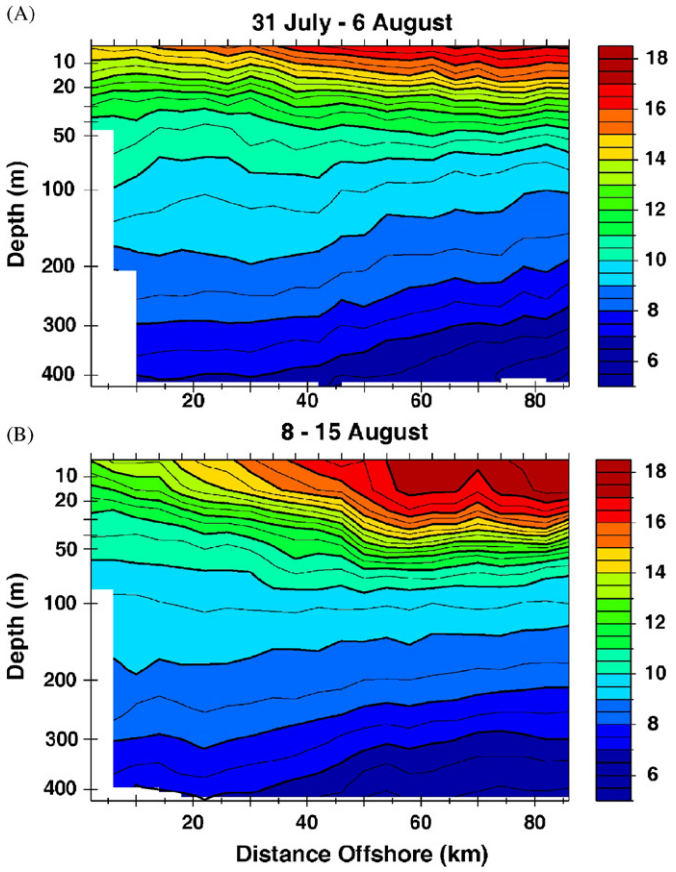

Fig. 10. Alongshore and time-averaged temperature measurements (°C) averaged in 10-m depth bins and 4-km bins of offshore distance (shortest distance to the coast) for (A) July 31 though August 6, 2006 and (B) August 8–15, 2006. The view is southward with the coast on the left.

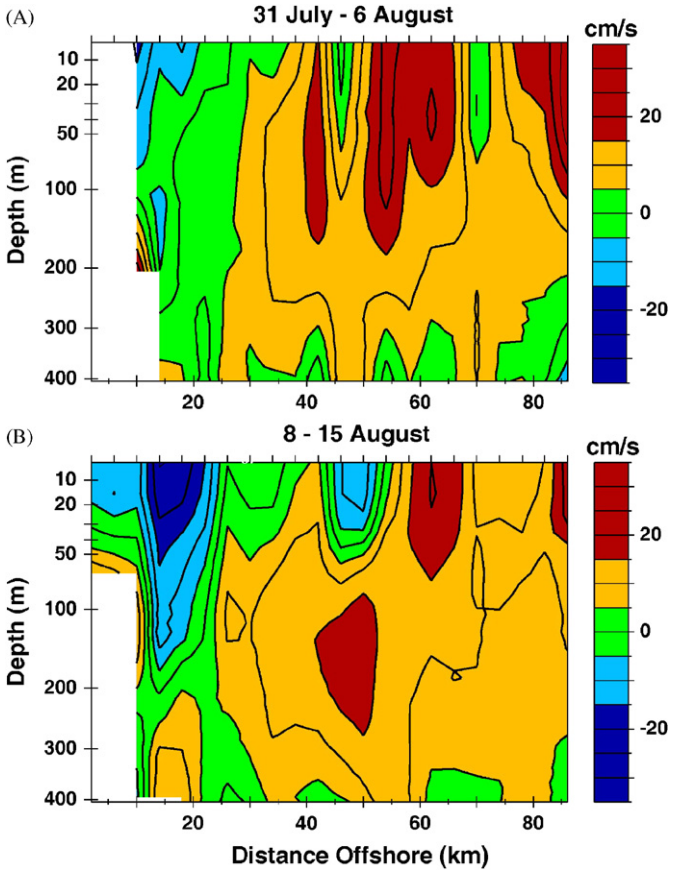

Fig. 11. Absolute alongshore velocity (cm/s) averaged over (A) July 31 through August 6, 2006 and (B) August 8–15, 2006. Geostrophic shear (from T and S sections like Fig. 10) was referenced by the alongshore-averaged glider-measured depth-averaged velocity (from Fig. 9). Since this constrains the vertical integral of velocity, 400 m is not a reference level and the velocities there are not weak by construction. The velocity scale is at right with positive numbers poleward and negative equatorward. The view is southward with the coast on the left.

temporally lagged correlation of nearly co-located temperature measurements and the horizontally isotropic spatially lagged correlation of nearly simultaneous measurements at the same depth based on all glider, shipboard, and mooring data from AOSN-II.

Several aspects of the measured scale structure deserve comment. First, the spatial and temporal 1/e-folding scales of 15 km and 2 days, respectively, are nearly a factor of 10 smaller than the scales of typical deep-water mesoscale eddies, which are commonly 100 km and 30 days. Second, the correlation values appear to increase rapidly as both the spatial and temporal separations become small. Indeed, at the smallest separations of 0.5 days and 5 km the correlation is about 0.8, suggesting that 20% of the observed temperature variance has smaller scales than this. Third, the correlation shapes are approximately the same for all depths shown (and all others that are not shown). A more complete discussion of the statistics of the AOSN-II variability is given by Davis et al. (2009) but the main point is that the results in Fig. 12 show that the sampling array for the five offshore Spray gliders was too thin to map any but the largest-scale components of the observed fields.

4.4. Multi-scale regional dynamics

The multi-scale dynamical interaction between the large-scale and mesoscale variabilities of the August 2003 circulation and their relationship with the upwelling-related events have been investigated using the methodology multi-scale energy and vorticity analysis (MS-EVA), and the MS-EVA-based localized instability theory developed by Liang and Robinson (2005, 2007). MS-EVA is built on the basis of the multi-scale window transform, a recently established mathematical apparatus by Liang and Anderson (2007). In this framework, the multi-scale processes in a given functional space are represented on its *scale windows*, or mutually orthogonal sub-spaces, each with an exclusive range of time scales. The objective of the MS-EVA is, accordingly, to investigate how energy and enstrophy are transported within their individual scale windows, redistributed through the interaction between the windows, and converted and dissipated when a system is steered forward. The redistribution is characterized by a concept called *perfect transfer*, which has been rigorously connected to the two important processes, barotropic instability and baroclinic instability, in geophysical fluid dynamics.

The AOSN-II Harvard Ocean Prediction System (HOPS) model fields have been analyzed in three mutually exclusive time sub-spaces: a large-scale window (>8 days), a mesoscale window (0.5–8 days), and a sub-mesoscale window (<0.5 days). The analysis has been performed during the upwelling–relaxation–upwelling cycle of winds shown in Fig. 2. Upwelling-favorable winds occur from 6–19 August to 23–31 August and the relaxation period is 19–22 August. The dynamics of the fields are driven externally by wind and surface fluxes and are characterized internally by the transfers of available potential energy (APE) and kinetic energy (KE) from the large scale to the mesoscale both (i) during upwelling and (ii) during relaxation. Off of Point Sur the wind destabilizes the system directly during upwelling, with wind

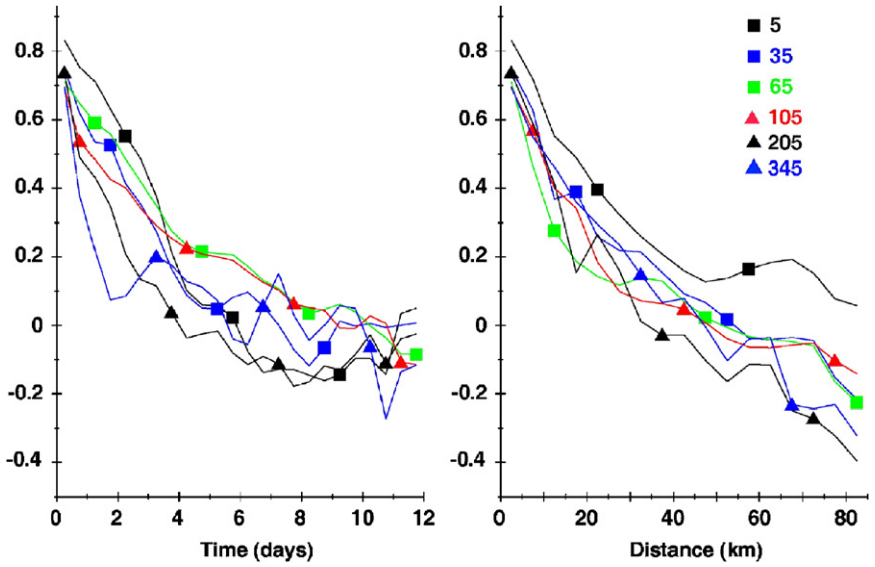

Fig. 12. Temporally lagged correlation (left) and spatially lagged isotropic correlation (right) of temperature at various depths. Temporally lagged result includes all AOSN-II observations that are within 5 km of each other while spatially lagged correlation includes all data whose observation time differs by less than 12 h. The smallest lag bins do not include data correlated with themselves. The legend at upper right describes the color and symbol code for different depths in meters.

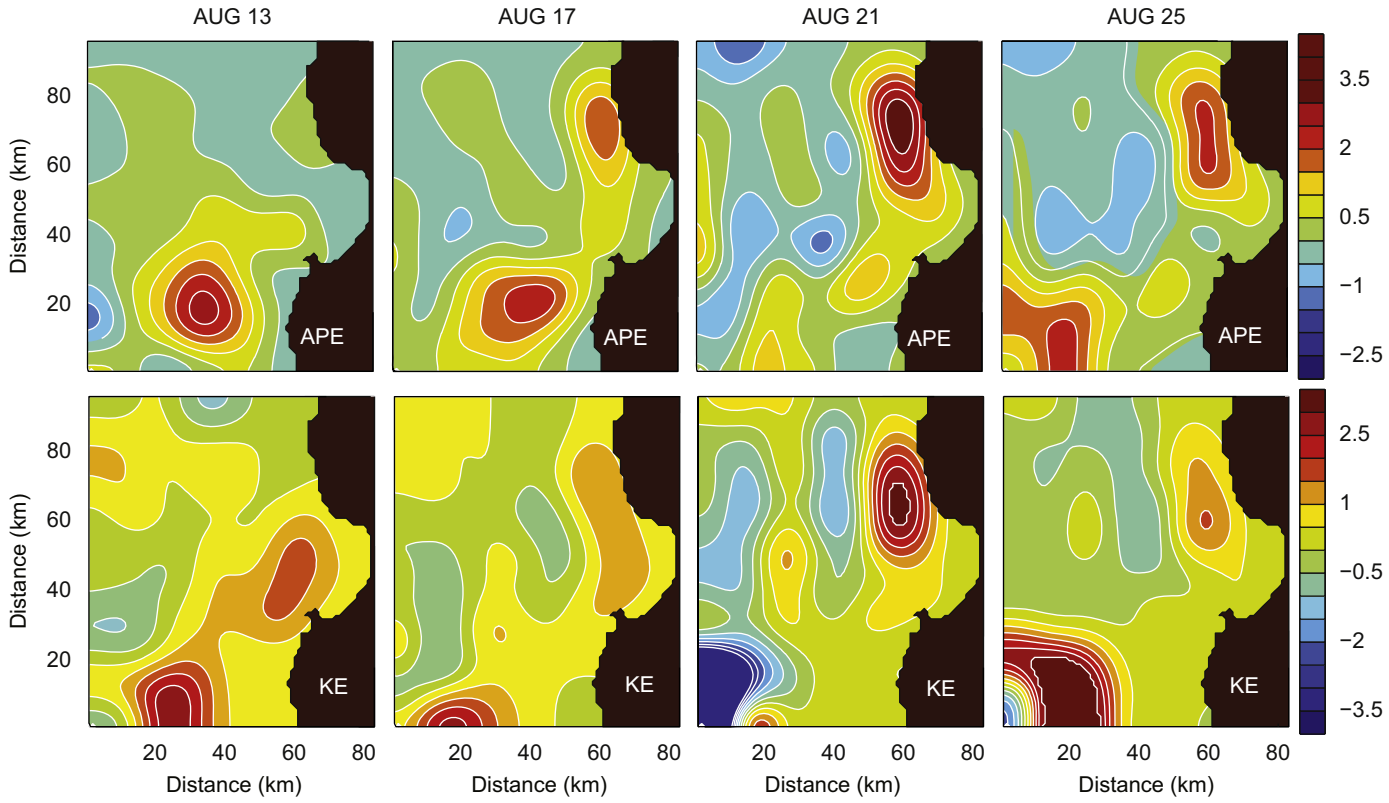

Fig. 13. Energy *transfer* term from the HOPS large-scale window to mesoscale window at 10 m. Top row—available potential energy (APE); bottom row—kinetic energy (KE).

energy captured within the large-scale window and continually released to the mesoscale. In contrast, near and in Monterey Bay, the wind tends to stabilize the southward coastal current, energy is stored in the large scale, and instability occurs only when the external wind constraint is relaxed.

Fig. 13 illustrates the available potential and kinetic energy transfer from the large-scale window to the mesoscale window at 4 day intervals from 13 to 25 August and Fig. 14 schematizes the energy transfer process. During (i) upwelling (13, 17, and 25 August) the greatest direct transfer of APE and KE is in the area to the west of Point Sur. Once (ii) relaxation occurs (21 August), energy transfer in this location is significantly reduced and the location of energy transfer moves to the region north of Monterey Bay, near Point Ano Nuevo. The generated mesoscale structures propagate northward along the coast with dispersion properties similar to those of free thermocline-trapped, coastally trapped

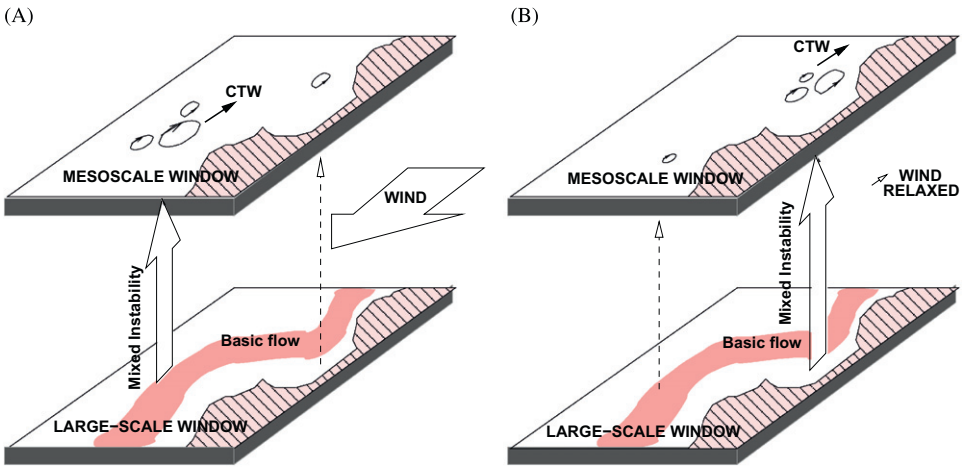

Fig. 14. Schematic of the major dynamical processes in the upper layer near Monterey Bay during (A) upwelling-favorable winds and (B) relaxation. Major energy transfer from the large-scale window to the mesoscale window takes place west of Point Sur during upwelling, while, during relaxation, major energy transfer takes place north of and in Monterey Bay. The generated mesoscale events propagate northward in the form of coastally trapped waves.

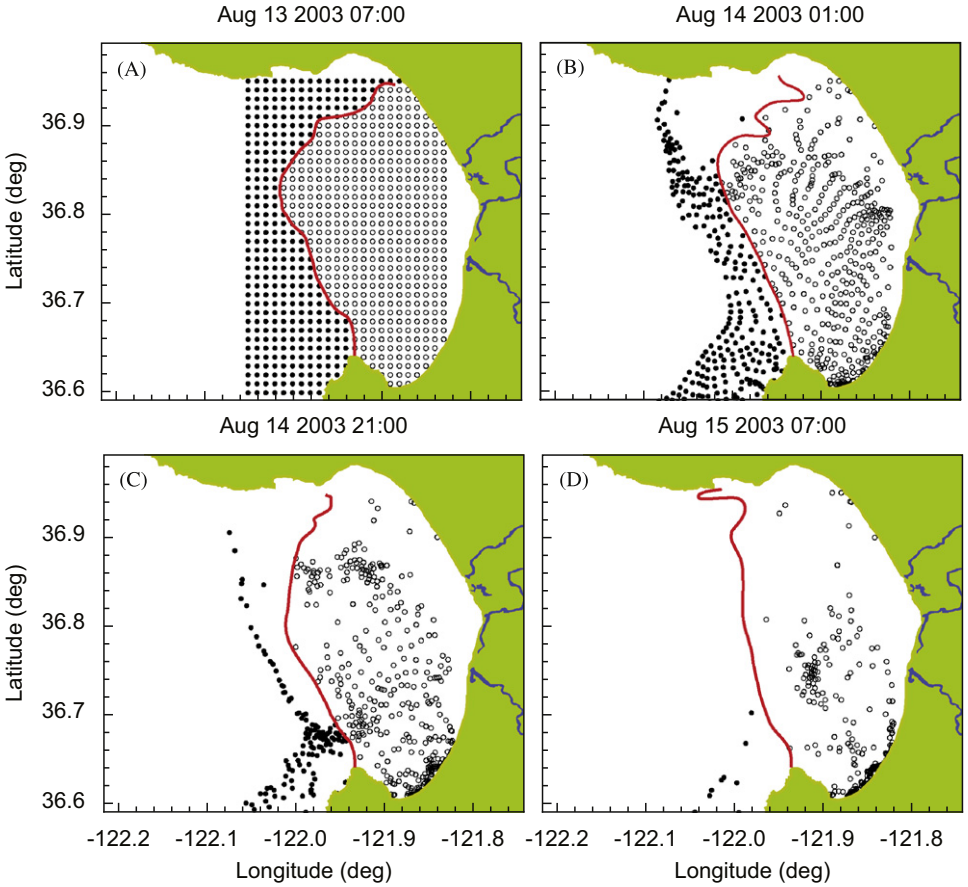

Fig. 15. Four snapshots of particle dispersion in the Monterey Bay in the vicinity of an LCS (red line) during upwelling favorable winds. The LCS and particle dispersion were computed from pseudo-drifters inserted into the CODAR HF radar surface current maps obtained during the AOSN-II experiment. Results are shown for (A) August 13, 2003 at 0700; (B) August 14, 2003 at 0100; (C) August 14, 2003 at 2100; and (D) August 15, 2003 at 0700. For additional discussion of this figure, see (Shadden et al., 2009).

waves. These waves have been previously observed off Point Sur by other investigators (Ramp et al., 1997).

4.5. *Lagrangian coherent structures in the Monterey Bay*

Lagrangian Coherent Structures, or LCS, is a computational technique for processing velocity field data in a flow, including currents in the ocean (Shadden et al., 2005). The basic methodology for this technique, based on the idea of finite time Liapunov exponents (measuring how particles are separating in forward time, or converging in backward time) originated during the few years before AOSN-II (Haller, 2002; Lekien, 2003) and was subsequently further developed using the AOSN-II data.

One of the things LCS can provide is to discern regions of different particle (or drifter) behavior. In conjunction with model

predictions, this can be a useful predictive tool. The interesting fact is that even in a complex flow such as that in Monterey Bay, LCS provides time-varying curves that separate particles that have different dynamical fates and particles do not cross these LCS. There is, for instance, a well-defined curve (technically, a repelling LCS) that separates particles in the inner bay from those in the outer bay (Fig. 15). Even though this curve is moving in time, and even though the flow is complex with multiple space and time scales, this curve on the scale of the bay itself sharply separates particles that have different fates. Particles on one side of the curve stay on that side. Thus, the fluid to the right of the red curve may be regarded, for this time period, to be re-circulating in the bay. That there even is such a well-defined curve is remarkable. Numerical evidence supports the idea that this curve (although perhaps not LCS for smaller-scale structures) is robust to data and model uncertainty.

Since the problem is time-varying, the recirculation zone does not persist indefinitely, and how such structures appear and disappear is related to the mechanisms of mixing and transport in the ocean. LCS can determine the boundaries of vortex regions and elucidate the mechanisms of entrainment and detrainment from vortex structures. It does so with greater clarity and precision than, for example, vorticity plots, as has been demonstrated in computations with laboratory vortex rings (Shadden et al., 2006). An example for the ocean has been computed using output from the JPL/ROMS model (Fig. 16). The fluid in the lobes, defined as the regions initially bounded by the LCS, was initially distributed as in Fig. 16B. Over time, the fluid moved away from the repelling LCS (orange) and towards the attracting LCS (blue) ultimately being entrained by the blue vorticies as shown in Figs. 16C and D. Transport and mixing occurs via the motion of the lobes since no fluid crosses the LCS. That drifters in the green lobes are flushed out to sea while drifters in the brown lobes recirculate near the coast evinces the property that LCS separate regions with different particle fates and residence times. This makes LCS a very promising tool for studying the distribution of water-mass properties, determining the fate of pollutants and oil spills, and planning how to seed surface drifters and autonomous vehicles for field studies of ocean dynamics.

4.6. Ocean-leaving radiance

The ocean-leaving radiance data were sometimes helpful in delineating the water-mass boundaries in addition to showing the distribution of marine organisms, particularly during weak winds

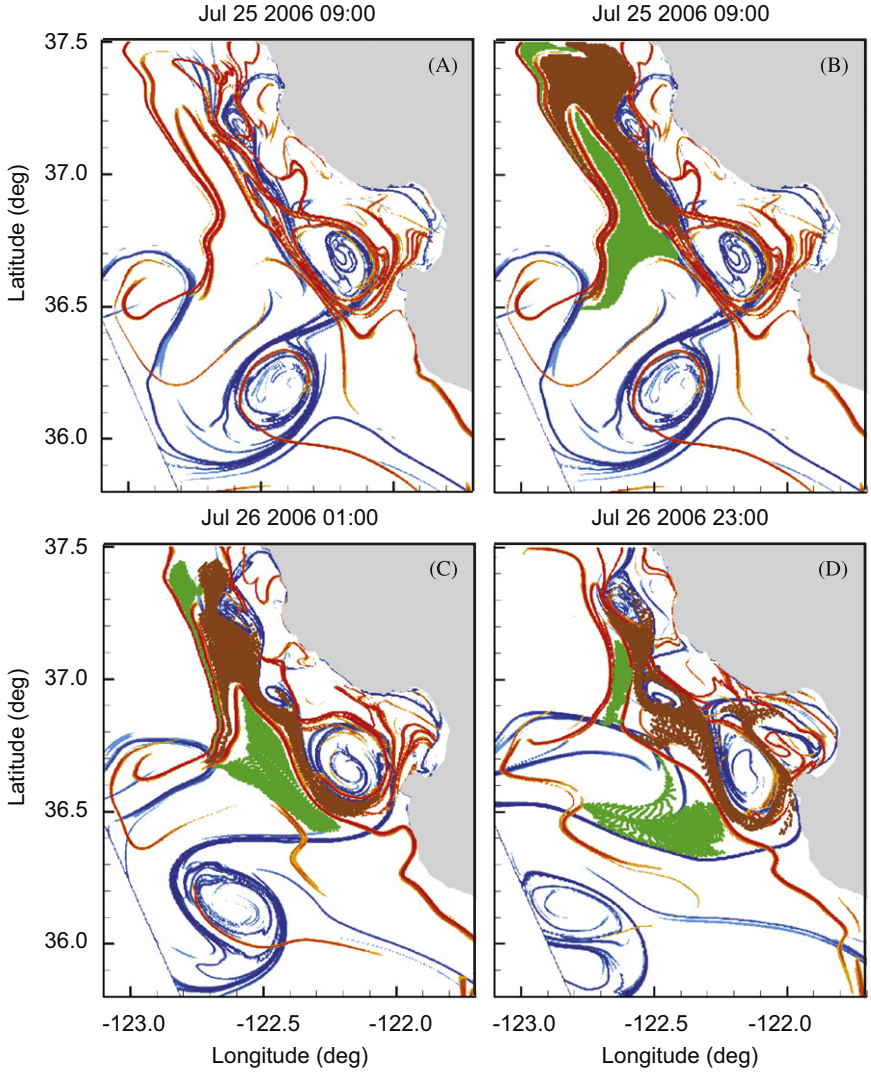

Fig. 16. LCS along the central California coast near the Monterey Bay as computed from the JPL/ROMS model output. The LCS are depicted for (A and B) July 25, 2006 at 0900, (C) July 26, 2006 at 0100, and (D) July 26, 2006 at 2300. Intersections of the attracting LCS (blue curves) and the repelling LCS (orange curves) define the boundaries of lobes colored green and brown.

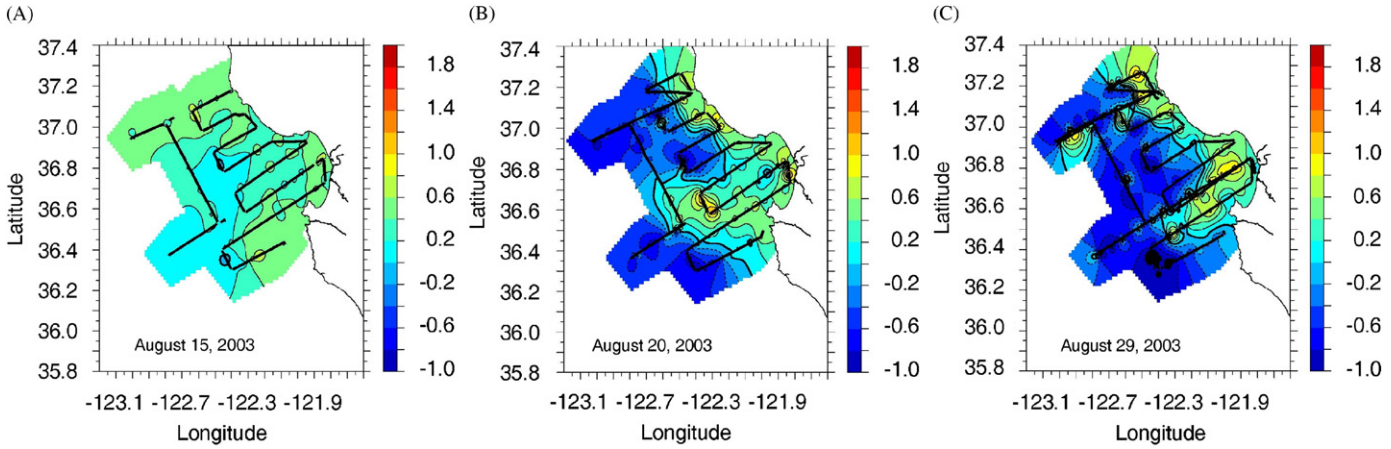

Fig. 17. Chlorophyll-*a* distributions as sensed from the hyperspectral sensor on board the TWIN OTTER aircraft for (A) August 15, (B) August 20, and (C) August 29, 2003.

when a thin layer of warm surface water masked the underlying structures. The hyperspectral data were collected using a HOBI Labs HydroRad hyperspectral radiometer measuring downwelling irradiance (E_d), upwelling radiance (L_u), and downwelling radiance (L_d). From these parameters, the water-leaving radiance (L_w) was calculated using different algorithms for a cloud-covered or cloud-free sky as appropriate. The water-leaving radiance from four spectral channels was combined subsequently to estimate the chlorophyll-*a* (Chl-*a*) content of the surface water using the SeaWiFS OC4 version 4 algorithm. Details of the calculations can be found in a separate technical report (Anderson and Ramp, 2005).

Three examples of the surface distributions of Chl-*a* from 15, 20, and 29 August were sampled during the first upwelling event, the wind relaxation, and the second upwelling event (Fig. 17). Comparison with Figs. 5G, H, and L shows almost no Chl-*a* seaward of the 17 °C isotherm, which may be taken as the boundary between the California Current water and the coastal water. The exception was an offshore patch of high chlorophyll near 36.9°N, 123.0°W on 29 August, which according to SST (see Fig. 5K) was located in old upwelled water which had been previously advected offshore on 25 August. All the Chl-*a* maps were patchier than SST with the highest values occurring away from the coast in older upwelled water. The vigorous advection and mixing during active upwelling events apparently prohibited the static stability required for a phytoplankton bloom to take place. Once the wind died down and surface warming re-stratified the water column, growth accelerated rapidly. The offshore "squirt" south of the bay (Fig. 5H) contained patches of high Chl-*a* water being advected offshore from Point Pinos by the eddy identified by the gliders. The Chl-*a* distributions on 15 and 29 August show the greater offshore advection of material during the earlier event vs. the later one. The nearly oligotrophic water close to shore off Año Nuevo on 29 August (dark blue in Fig. 17C) further supports the notion that the California Current confined the upwelling center to the nearshore region during the second event and encouraged the southward, rather than offshore advection of the cold, nutrient-rich water.

5. Impacts and conclusions

The AOSN-II experiment successfully demonstrated the viability of several new technologies and techniques in addition to illuminating some basic scientific issues surrounding coastal upwelling off central California. Gliders running closed cells and racetracks were able to determine robust statistics of the flow due to their impressive persistence and spatial coverage. They also observed smaller-scale features such as the eddy at the mouth of the Monterey Bay. Gliders flying formations were able to sample frontal gradients in both the horizontal and vertical while moving across or against the flow field as well as moving with it. These observations were not previously possible with floats or drifters, and were not possible without an impressive level of autonomous control over the small glider fleets. The low-flying aircraft was able to map out the three-dimensional structure of the wind fields with a level of detail sufficient to make quantitative comparisons with the latest high-resolution atmospheric models. By flying beneath the clouds, the aircraft also collected a time series of synoptic snapshots of the surface temperature and ocean-leaving radiance fields that were not available any other way. The SST was a key parameter for assimilation into all three numerical models on a daily basis. The Lagrangian Coherent Structures (LCS) analysis technique, relatively new to the field of oceanography, showed great promise for understanding the flow dynamics and particle fates, whether using observational data (surface current maps from HF radar) or numerical model (JPL/ROMS) output.

Using the combined power of these new methodologies, the following picture of the circulation in and around the Monterey Bay during a series of upwelling and relaxation events has emerged. Two upwelling events were observed, one lasting 14 days and the second nine, with a 3-day relaxation event in between. The wind speed was similar between the two upwelling events, blowing steadily from the northwest at 10–15 m/s. During the relaxation winds were poleward at about 5 m/s. All three events were well sampled by the aircraft, gliders, and ships.

Both upwelling events began when a pool of cold water less than 13 °C appeared at the surface off Cape Año Nuevo. As the wind continued to blow for about 5 days, the cold pool expanded and spread offshore and to the south across the mouth of the Monterey Bay. A key difference between the two events was the degree of offshore spreading: The first event spread offshore and to the south while the second event spread exclusively to the south. Both models and observations indicate that the key difference between these events was caused by the position of the offshore meanders and eddies of the California Current System. During the intervening relaxation event, the boundary between the coastal and CCS waters, as indicated by the 17 °C isotherm and the Chl-*a* content, moved 40 km onshore to within 5 km of the coast at its closest incursion. This frontal zone effectively blocked the offshore advection of cold water during the second upwelling event, and the equatorward geostrophic flow along the front aided the southward advection of the cold water by the wind. The plume thinned vertically as it moved southward

across the bay to less than 30 m at the southern side. The dynamics of the eddy/frontal movements remains a mystery as they were not always correlated with the local wind stress. While the front clearly moved onshore during the relaxation, it also moved onshore at other times and did not retreat offshore during the second upwelling event. Using the entire glider data set, the temporally and spatially lagged data indicate e-folding scales of 2 days and 15 km, respectively for these eddies, much smaller than the scales (30 days and 100 km) typically observed in deep-water eddies offshore. The California Undercurrent was present in approximately the same location throughout the experiment, further offshore in the north than the south. The changes in the vertically averaged currents were due primarily to changes in the upper water column rather than changes in the CUC.

These results suggest directions for future dynamical studies. The spatial distribution of the wind-stress curl suggests that positive curl on the inshore side of a sub-mesocale atmospheric jet may be important in driving upwelling in the Monterey Bay, in addition to divergence at the coast. The HOPS model suggests that the energy transfer from the large scale to the mesoscale takes place via mixed barotropic/baroclinic instability off Point Sur during upwelling events and in the northern Monterey Bay during relaxations. More focused observational studies are needed to verify these ideas.

Acknowledgments

The authors are indebted to the Office of Naval Research, Ocean, Atmosphere, and Space Department, for funding the AOSN program. Dr. Tom Curtin of ONR provided direction and leadership for the AOSN program over a period of many years to make it a reality. Additional support, especially for shore-side logistics, was provided by the Monterey Bay Aquarium Research Institute. Aircraft support was provided by the NPS Center for Interdisciplinary Remotely Piloted Aircraft Studies (CIRPAS), especially by Bob Bluth, Haf Jonsson, and Gintas Buzorius. Countless technical staff and graduate students worked long hours during the field program to collect and process real-time data, implement models and assimilate the data, and to disseminate and discuss the results.

References

Anderson, T.E., Ramp, S.R., 2005. Chlorophyll and water-leaving radiances from an airborne spectral radiometer in the Monterey Bay. In: 52nd Eastern Pacific Ocean Conference, Fallen Leaf Lake, CA, September 27–30, 2005.

Anon. 2002. Management and scientific informational needs for harmful algal bloom and fisheries forecasting in the Gulf of Maine. In: Proceedings of the ECOHAB/GLOBEC Gulf of Maine Modeling Workshop. NOAA Center for Sponsored Coastal Ocean Research (CSCOR), Portland, Maine, June 17–18, 2002.

Anon., 2005. Workshop on planning coordinated research on ecosystems, climate and policy in the Northeast. Cooperative Institute for Climate and Ocean Research (CICOR), Woods Hole Oceanographic Institution, and the Northeast Fisheries Science Center (NMFS), January 11–13, 2005. 〈www.whoi.edu/science/cicor/workshop05/report.html〉.

Barth, J.A., Wheeler, P.A., 2005. Introduction to special section: coastal advances in shelf transport. J. Geophys. Res., doi:10.1029/2005JC003124.

Bellingham, J., Robinson, A., Davis, R.E., Leslie, W., Chao, Y., Fratantoni, D., Leonard, N., Ramp, S.R., Paduan, J.D., Haddock, S.H.D., Chavez, F.P., Thomas, H., 2009. Engineering coastal observation and prediction systems. Deep-Sea Res. II, this issue.

Besiktepe, S.T., Lermusiaux, P.F.J., Robinson, A.R., 2003. Coupled physical and biogeochemical data driven simulations of Massachusetts Bay in late summer: real-time and post-cruise data assimilation. J. Mar. Systems 40, 171–212.

Bogden et al., 2001. Gulf of Maine Ocean Observing System (GOMOOS). See 〈www.gomoos.org〉.

Bovio, E., Tyce, R., Schmidt, H. (Eds.), 2003. Rapid environmental assessment. NATO SACLANT Undersea Research Centre, SACLANTCEN Conference Proceedings Series CP-46.

Breaker, L.C., Mooers, C.N.K., 1986. Oceanic variability off the central California coast. Progr. Oceanogr. 17, 61–135.

Bretherton, F.P., Davis, R.E., Fandry, C.B., 1975. A technique for objective analysis and design of oceanographic experiments. Deep-Sea Res. 23, 559–582.

Brink, K.H., Beardsley, R.C., Niiler, P.P., Abbott, M.R., Huyer, A., Ramp, S.R., Stanton, T.P., Stuart, D., 1991. Statistical properties of near surface flow in the California coastal transition zone. J. Geophys. Res. 96, 14,693–14,706.

Chao,Y., Li, Z., Farrara, J., McWilliams, J.C., Bellingham, J., Capet, X., Chavez, F., Choi, J.-K., Davis, R., Doyle, J., Frantaoni, D., Li, P., Marchesiello, P., Moline, M.A., Paduan, J., Ramp, S., 2009. Development, implementation and evaluation of a data-assimilative ocean forecasting system off the central California coast. Deep-Sea Research II, this issue [doi:10.1016/j.dsr2.2008.08.011].

Chelton, D.B., 1984. Seasonal variation of alongshore geostrophic velocity off central California. J. Geophys. Res. 89, 3473–3486.

Davis, R.E., Eriksen, C.E., Jones, C.P., 2002. Autonomous buoyancy-driven underwater gliders. In: Griffiths, G. (Ed.), The Technology and Applications of Autonomous Underwater Vehicles. Taylor & Francis, London, pp. 37–58 (324pp.).

Davis, R.E., Zhang, Y., Fratantoni, D., Bellingham, J., Chavez, F.P., McManus, M., Ramp, S.R., 2009. A statistical description of coastal variability. Deep-Sea Res. II, this issue.

deYoung, B., Heath, M., Werner, F., Chai, F., Megrey, B., Monfray, P., 2004. Challenges of modeling ocean basin ecosystems. Science 304, 1463–1466.

Dickey, T., 2003. Emerging ocean observations for interdisciplinary data assimilation systems. J. Mar. Systems 40–41, 5–48.

Doyle, J.D., Jiang, Q., Chao, Y., Farrara, J., 2009. High-resolution real-time modeling of the marine atmospheric boundary layer in support of the AOSNII field campaign. Deep-Sea Research II, this issue [doi:10.1016/j.dsr2.2008.08.009].

Edson, J., et al., 1999. Coupled marine Boundary layers and air–sea interaction initiative (CBLAST): combining process studies, simulations, and numerical models. Workshop Report.

Edson, J., Crawford, T., Crescenti, J., Farrar, T., Frew, N., Gerbi, G., Helmis, C., Hristov, T., Khelif, D., Jessup, A., Jonsson, H., Li, M., Mahrt, L., McGillis, W., Plueddemann, A., Shen, L., Skyllingstad, E., Stanton, T., Sullivan, P., Sun, J., Trowbridge, J., Vickers, D., Wang, S., Wang, Q., Weller, R., Wilkin, J., Yu, D., Zappa, C., 2006. The Coupled Boundary Layers and Air–Sea Transfer Experiment in Low Winds (CBLAST-LOW). Bulletin of the American Meteorological Society.

Fiorelli, E., Leonard, N.E., Bhatta, P., Paley, D.A., Bachmayer, R., Fratantoni, D.M., 2006. Multi-AUV control and adaptive sampling in Monterey Bay. IEEE/J. Ocean. Eng. 31, 935–948.

Graham, W.M., 1993. Spatio-temporal scale assessment of an ‘‘upwelling shadow’’ in northern Monterey Bay, California. Estuaries 16, 83–91.

Graham, W.M., Largier, J.L., 1997. Upwelling shadows as nearshore retention sites: the example of northern Monterey Bay. Cont. Shelf Res. 17, 509–532.

Haley Jr., P.J., Lermusiaux, P.F.J., Robinson, A.R., Leslie, W.G., Logoutov, O., Cossarini, G., Liang, X.S., Moreno, P., Ramp, S.R., Doyle, J.D., Bellingham, J., Chavez, F., Johnston, S., 2009. Forecasting and reanalysis in the Monterey Bay/California Current region for the Autonomous Ocean Sampling Network-II experiment. Deep-Sea Research II, this issue [doi:10.1016/j.dsr2.2008.08.010].

Haller, G., 2002. Lagrangian coherent structures from approximate velocity data. Phys. Fluids A 14, 1851–1861.

Kalogiros, J., Wang, Q., Ramp, S., Buzorius, G., Jonnsson, H., 2006. Aircraft observations of marine boundary layer structure in the area of Monterey Bay. In: Proceedings, 17th Symposium on Boundary Layers and Turbulence, American Meteorological Society, San Diego, CA, 22–25 May, 5pp.

Lekien, F., 2003. Time-dependent dynamical systems and geophysical flows. Ph.D. Thesis, Caltech.

Lentz, S.J., 1987. A description of the 1981 and 1982 spring transitions over the northern California shelf. J. Geophys. Res. 92, 1545–1567.

Leonard, N.E., Paley, D., Lekien, F., Sepulchre, R., Fratantoni, D.M., Davis, R.E., 2007. Collective motion, sensor networks and ocean sampling. Proc. IEEE 95 (1).

Lermusiaux, P.F.J., 1999. Estimation and study of mesoscale variability in the Strait of Sicily. Dyn. Atmos. Oceans 29, 255–303.

Lermusiaux, P.F.J., 2001. Evolving the subspace of the three-dimensional multiscale ocean variability: Massachusetts Bay. J. Mar. Systems 29/1–4, 385–422.

Lermusiaux, P.F.J., 2007. Adaptive modeling, adaptive data assimilation and adaptive sampling. Physica D 230, 172–196.

Lermusiaux, P.F.J., Malanotte-Rizzoli, P., Stammer, D., Carton, J., Cummings, J., Moore, A.M., 2006. Progress and prospects of US data assimilation in ocean research. Oceanography 19 (1), 172–183.

Liang, X.S., Anderson, D.G.M., 2007. Multiscale window transform. SIAM J. Multiscale Model. Simul. 6, 437–467.

Liang, X.S., Robinson, A.R., 2005. Localized multiscale energy and vorticity analysis. I. Fundamentals. Dyn. Atmos. Oceans 38 (3–4), 195–230.

Liang, X.S., Robinson, A.R., 2007. Localized multiscale energy and vorticity analysis. II. Finite-amplitude instability theory and validation. Dyn. Atmos. Oceans 44, 51–76.

Lynch, D.R., Davies, A.M. (Eds.), 1995. Quantitative Skill Assessment for Coastal Ocean Models, Coastal and Estuarine Studies, vol. 47. American Geophysical Union, Washington, DC, pp. 153–174.

Lynch, D.R., Naimie, C.E., Ip, J.T., Lewis, C.V., Werner, F.E., Luettich, R., Blanton, B.O., Quinlan, J., McGillicuddy Jr., D.J., Ledwell, J.R., Churchill, J., Kosnyrev, V., Davis, C.S., Gallager, S.M., Ashjian, C.J., Lough, R.G., Manning, J., Flagg, C.N., Hannah, C.G., Groman, R.C., 2001. Real-time data assimilative modeling on Georges Bank. Oceanography 14 (1), 65–77 〈http://wwwnml.dartmouth.edu/Publications/externalpublications/PUB-99-2/〉.

Moline, M.A., Blackwell, S.M., Allen, B., Austin, T., Forrester, N., Goldsborogh, R., Purcell, M., Stokey, R., vonAlt, C., 2005. Remote Environmental Monitoring

UnitS (REMUS) An autonomous vehicle for characterizing coastal environments. J. Atmos. Ocean. Tech. 22, 1797–1808.
Mooers, C.N.K. (Ed.), 1999. Coastal Ocean Prediction, AGU Coastal and Estuarine Studies Series. American Geophysical Union.
Mooers, C., Meinen, C., Baringer, M., Bang, I., Rhodes, R., Barron, C., Bub, F., 2005. Cross validating ocean prediction and monitoring systems. Eos Trans. AGU 86 (29), 269.
Nelson, C.S., 1977. Wind stress and wind stress curl over the California Current. NOAA Technical Report NMFS SSRF-714, US Department of Commerce, NOAA/NMFS, 89pp.
Noble, M.A., Ramp, S.R., 2000. Subtidal currents over the central California slope: evidence for offshore veering of the undercurrent and for direct, wind-driven slope currents. Deep-Sea Res. II 47, 871–906.
Ocean.US, 2002. An Integrated and Sustained Ocean Observing System (IOOS) for the United States: Design and Implementation. Ocean.US, Arlington, VA, (21pp.).
Ocean.US, 2004. Regional Organizational Workshop: Building Regional Capability for the IOOS. OceanUS Publication No. 5. Ocean.US, Arlington, VA, (28pp.).
Onken, R., Robinson, A.R., Lermusiaux, P.F.J., Haley Jr., P.J., Anderson, L.A., 2002. Data-driven simulations of synoptic circulation and transports in the Tunisia–Sardinia–Sicily region. J. Geophys. Res. 108 (C9), 8123–8136.
Onken, R., Robinson, A.R., Kantha, L., Lozano, C.J., Haley, P.J., Carniel, S., 2005. A rapid response nowcast/forecast system using multiply-nested ocean models and distributed data systems. J. Mar. Systems 56, 45–66.
Paduan, J.D., Cook, M.S., 1997. Mapping surface currents in Monterey Bay with CODAR-type HF radars. Oceanography 10, 49–52.
Paduan, J.D., Rosenfeld, L.K., 1996. Remotely sensed surface currents in Monterey Bay from shore-based HF radar (Coastal Ocean Dynamics Application Radar). J. Geophys. Res. 101, 20,669–20,686.
Paduan, J., Shulman, I., 2004. HF radar data assimilation in the Monterey Bay area. J. Geophys. Res. 109, CO7S09.
Pierce, S.D., Smith, R.L., Kosro, P.M., Barth, J.A., Wilson, C.D., 2000. Continuity of the poleward undercurrent along the eastern boundary of the mid-laititude north Pacific. Deep-Sea Res. II 47, 811–829.
Pinardi, N., Woods, J.D. (Eds.), 2002. Ocean Forecasting: Conceptual Basis and Applications. Springer, Berlin.
Ramp, S.R., Abbott, C.L., 1998. The vertical structure of currents over the continental shelf off point Sur, CA, during spring 1990. Deep-Sea Res. II 45, 1443–1470.
Ramp, S.R., Rosenfeld, L.K., Tisch, T.D., Hicks, M.R., 1997. Moored observations of the current and temperature structure over the continental slope off central California, 1, A basic description of the variability. J. Geophys. Res. 102, 22,877–22,902.
Ramp, S.R., Paduan, J.D., Shulman, I., Kindle, J., Bahr, F.L., Chavez, F.P., 2005. Observations of upwelling and relaxation events in the northern Monterey Bay during August 2000. J. Geophys. Res. 110, C07013, (21pp.).
Robinson, A.R., 1999. Forecasting and simulating coastal ocean processes and variabilities with the Harvard Ocean Prediction System. In: Mooers, C.N.K. (Ed.), Coastal Ocean Prediction. AGU Coastal and Estuarine Studies Series, 77–100. American Geophysical Union.
Robinson, A.R., Glenn, S.M., 1999. Adaptive sampling for ocean forecasting. Nav. Res. Rev. 51 (2), 28–38.
Robinson A.R., Lermusiaux, P.F.J., 2002. Data assimilation for modeling and predicting coupled physical–biological interactions in the sea. In: Robinson A.R., McCarthy, J.R., Rothschild, B.J. (Eds.), The Sea, vol. 12: Biological–Physical Interactions in the Ocean, pp. 475–536.
Robinson, A.R. and the LOOPS group, 1999. Real-time forecasting of the multidisciplinary coastal ocean with the Littoral Ocean Observing and Predicting System (LOOPS). In: Third Conference on Coastal Atmospheric and Oceanic Prediction and Processes, 3–5 November 1999. American Meteo. Soc., New Orleans, LA, pp. 30–35.
Robinson, A.R., Lermusiaux, P.F.J., Sloan III, N.Q., 1998. Data assimilation. In: Brink, K.H., Robinson, A.R. (Eds.), The Sea: The Global Coastal Ocean I, Processes and Methods, vol. 10. Wiley, New York, NY, pp. 541–594.
Robinson, A.R., Sellschopp, J., Warn-Varnas, A., Leslie, W.G., Lozano, C.J., Haley Jr., P.J., Anderson, L.A., Lermusiaux, P.F.J., 1999. The Atlantic Ionian stream. J. Mar. Systems 20, 129–156.
Robinson A.R., Sellschopp, J., Leslie, W.G., Alvarez, A., Baldasserini, G., Haley, P.J., Lermusiaux, P.F.J., Lozano, C.J., Nacini, E., Onken, R., Stoner, R., Zanasca, P., 2003. Forecasting synoptic transients in the Eastern Ligurian Sea. In: Bovio, E., Tyce, R., Schmidt, H. (Eds.), Rapid Environmental Assessment. SACLANTCEN.
Rosenfeld, L.K., Schwing, F.B., Garfield, N., Tracy, D.E., 1994. Bifurcated flow from an upwelling center: a cold water source for Monterey Bay. Cont. Shelf Res. 14, 931–964.
Runge, J., 2005. Modeling needs related to the Regional Observing System in the Gulf of Maine. RARGOM Report 05-1
Schofield, T., Bergmann, P., Bissett, J.F., Grassle, D., Haidvogel, J., Kohut, M., Moline, S.M., Glenn, A., 2002. The long-term ecosystem observatory: an integrated coastal observatory. IEEE J. Ocean. Eng. 27, 146–154.
Shadden, S.C., Lekien, F., Marsden, J.E., 2005. Definition and properties of Lagrangian coherent structures from finite-time Lyapunov exponents in two-dimensional aperiodic flows. Physica D 212, 271–304.
Shadden, S.C., Dabiri, J.O., Marsden, J.E., 2006. Lagrangian analysis of fluid transport in empirical vortex ring flows. Phys. Fluids 18, (047105-1–047105-11).
Shadden, S.C., Lekien, F., Paduan, J.D., Chavez, F., Marsden, J.E., 2009. The correlation between surface drifters and coherent structures based on HF radar in Monterey Bay. Deep-Sea Research II, this issue [doi:10.1016/j.dsr2.2008.08.008].
Shchepetkin, A.F., McWilliams, J.C., 2004. The Regional Oceanic Modeling System: a split-explicit, free-surface, topography-following-coordinate ocean model. Ocean Modelling 9, 347–404.
Sherman, J., Davis, R.E., Owens, W.B., Valdes, J., 2001. The autonomous underwater glider 'Spray'. IEEE Ocean. Eng. 26, 437–446.
Shulman, I., Paduan, J.D., 2009. Assimilation of HF radar-derived radials and total currents in the Monterey Bay area. Deep-Sea Research II, this issue [doi:10.1016/j.dsr2.2008.08.004].
Shulman, I., Wu, C.R., Lewis, J.K., Paduan, J.D., Rosenfeld, L.K., Kindle, J.C., Ramp, S.R., Collins, C.A., 2002. High resolution modeling and data assimilation in the Monterey Bay area. Cont. Shelf Res. 22, 1129–1151.
Shulman, I., Kindle, J., Derada, S., Anderson, S., Penta, B., Martin, P., 2004. Development of hierarchy of different resolution models for study US West Coast California Current Ecosystem. In: Spaulding, M. L. (Ed.), Estuarine and Coastal Modeling, Proceedings of Eighth International Conference on Estuarine and Coastal Modeling, pp. 74–88.
Shulman, I., McGillicuddy Jr., D.J., Moline, M.A., Haddock, S.H.D., Kindle, J.C., Nechaev, D., Phelps, M.W., 2005. Bioluminescence intensity modeling and sampling strategy optimization. J. Atmos. Ocean. Tech. 22, 1267–1281.
Tisch, T.D., Ramp, S.R., Collins, C.A., 1992. Observations of the geostrophic current and water mass characteristics off Point Sur, California from May 1988 through November 1989. J. Geophys. Res. 97, 12,535–12,556.
Wang, Q., Kalogiros, J., Ramp, S.R., Paduan, J.D., Buzorius, G., Jonsson, H., 2007. Wind stress and coastal upwelling in the Monterey Bay observed during AOSN-II. J. Geophys. Res., submitted.
Wickham, J.B., Bird, A.A., Mooers, C.N.K., 1987. Mean and variable flow over the central California continental margin, 1978–1980. Cont. Shelf Res. 7, 827–849.
Wiebe, P.H, Beardsley, R.C., Bucklin, A.C., Mountain, D.G., (Eds.), 2001. Coupled biological and physical studies of plankton populations on Georges Bank and related North Atlantic regions. Deep-Sea Research 48 (1–3), 1–684.
Wilkin, J.L., Arango, H., Haidvogel, D.B., Sage Lichtenwalner, C., Glenn, S.M., Hedstrom, K.S., 2005. A regional ocean modeling system for the long-term ecosystem observatory. J. Geophys. Res. 110.
Winant, C.D., Beardsley, R.C., Davis, R.E., 1987. Moored wind, temperature, and current observations made during Coastal Ocean Dynamics Experiments 1 and 2 over the northern California continental shelf and upper slope. J. Geophys. Res. 92, 1569–1604.